

Design, Synthesis, Biological Evaluation, and Molecular Modeling Studies of TIBO-Like Cyclic Sulfones as Non-Nucleoside HIV-1 Reverse Transcriptase Inhibitors

Roberto Di Santo,^{*,[a]} Roberta Costi,^[a] Marino Artico,^[a] Rino Ragno,^[a] Antonio Lavecchia,^[b] Ettore Novellino,^[b] Enrico Gavuzzo,^[c] Francesco La Torre,^[d] Roberto Cirilli,^[d] Reynel Cancio,^[e] and Giovanni Maga^[e]

TIBO- and TBO-like sulfone derivatives 1 and 2 were designed, synthesized, and tested for their ability to block the replication cycle of HIV-1 in infected cells. The anti-HIV-1 activities of sulfones 3, which were intermediates in the syntheses of 1 and 2, were also evaluated. Surprisingly, the sulfone analogues of TIBO R82913 (compounds 1) were inactive, whereas interesting results were obtained for truncated derivatives 2. Compound 2w was the most potent among this series in cell-based assays ($EC_{50} = 0.07 \mu\text{M}$, $CC_{50} > 200 \mu\text{M}$, $SI > 2857$). It was twofold less potent than R82913, but more selective. An X-ray crystallographic analysis was carried out to establish the absolute configuration of 2w

and its enantiomer 2x, which were obtained by semipreparative HPLC of 2v, one of the most potent racemates. Compounds 1–3 were proven to target HIV-1 RT. In fact, representative derivatives inhibited recombinant HIV-1 RT in vitro at concentrations similar to those active in cell-based assays. 3D QSAR studies and docking simulations were developed on TIBO- and TBO-like sulfone derivatives to rationalize their anti-HIV-1 potencies and to predict the activity of novel untested sulfone derivatives. Predictive 3D QSAR models were obtained with a receptor-based alignment by docking of TIBO- and TBO-like derivatives into the NNBS of RT.

Introduction

Despite the considerable success of highly active antiretroviral therapy (HAART), AIDS remains one of the most urgent world health problems. In fact, the rapid emergence of drug-resistant HIV strains and severe side effects limit the efficacy of present therapies.^[1–3]

Currently, three different classes of chemotherapeutic agents are available to block the replication of HIV, the virus responsible for AIDS: reverse transcriptase inhibitors (RTIs),^[4] protease inhibitors (PRIs),^[5] and inhibitors of virus–cell fusion.^[6] RTIs are further grouped into two subclasses: nucleoside reverse transcriptase inhibitors (NRTIs), exemplified by zidovudine (AZT, Retrovir®), and non-nucleoside reverse transcriptase inhibitors (NNRTIs), such as nevirapine (Viramune®).^[7] Although structurally unrelated, all NNRTIs exert their antiviral effect through a noncompetitive mechanism by interacting with an allosteric site adjacent to the active site of the enzyme,^[8] which causes a distortion of the catalytic aspartate residues.^[9] It is well-known that NNRTIs assume a butterfly-like conformation within the enzyme binding site;^[10] the “wings” are usually composed of aromatic rings that interact with aromatic amino acid residues.

1-[(2-Hydroxyethoxy)methyl]-6-phenylsulfanylthymine (HEPT)^[11] and 4,5,6,7-tetrahydroimidazo[4,5,1-jk][1,4]benzodiazepin-2(1H)-one and -thione (TIBO)^[12] derivatives were the first compounds described within the NNRTI class. These were followed by nevirapine,^[7] efavirenz (Sustiva),^[13] and delavirdine

(Rescriptor),^[14] which have been approved for clinical use as AIDS therapeutics (Figure 1). As the above chemotherapeutic agents are not potent enough to completely eradicate HIV from patients of AIDS, or even to maintain long-term suppres-

[a] Prof. Dr. R. Di Santo, Prof. Dr. R. Costi, Prof. Dr. M. Artico, Dr. R. Ragno
Istituto Pasteur-Fondazione Cenci Bolognetti
Dipartimento di Studi Farmaceutici
Università degli Studi di Roma “La Sapienza”
P. le A. Moro 5, 00185 Roma (Italy)
Fax: (+39) 6-49913150
E-mail: roberto.disanto@uniroma1.it

[b] Prof. Dr. A. Lavecchia, Prof. Dr. E. Novellino
Dipartimento di Chimica Farmaceutica e Tossicologica
Università degli Studi di Napoli “Federico II”
Via D. Montesano 49, 80131 Napoli (Italy)

[c] Dr. E. Gavuzzo
Istituto di Chimica Biomolecolare, CNR sezione di Roma
P. le A. Moro 5, 00185 Roma (Italy)

[d] Dr. F. La Torre, Dr. R. Cirilli
Istituto Superiore di Sanità
Dipartimento del Farmaco
Viale Regina Elena 299, 00161 Roma (Italy)

[e] Dr. R. Cancio, Dr. G. Maga
Istituto di Genetica Molecolare IGM-CNR
Via Abbiategrasso 207, 27100 Pavia (Italy)

Supporting information for this article is available on the WWW under <http://www.chemmedchem.org> or from the author.

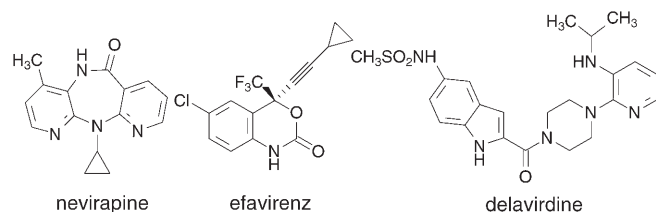


Figure 1. Structures of NNRTIs in current clinical use.

sion of virus replication and development of drug resistance, additional drugs should be developed.

Ever since the discovery of TIBO derivatives as noncompetitive inhibitors of reverse transcriptase (RT) that bind to a hydrophobic pocket close to the catalytic site,^[15] a number of structure–activity relationship (SAR),^[16–19] molecular modeling,^[20–22] and structural studies^[23] have been undertaken on this class of NNRTIs. The most potent TIBO derivative, R86183 (tivirapine),^[24] was not developed for clinical use primarily because its synthesis was too cumbersome. Extensive chemical modifications of this compound and its derivative, R82913, led to the 1,5-benzothiazepine derivatives^[25] and truncated analogues, tetrahydrobenzodiazepinones (TBO),^[25,26] which exhibited anti-HIV-1 activity, albeit at a much higher concentration than tivirapine (Figure 2).

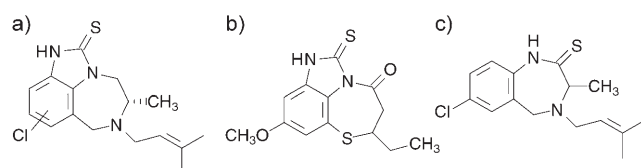


Figure 2. TIBO derivatives a) R82913 (9-Cl-TIBO), R86183 (8-Cl-TIBO, tivirapine) and b) 1,5-benzothiazepine; c) TBO.

The relevance of TIBO derivatives within the NNRTI class and recent reports of nitrophenyl phenylsulfones (NPPSs),^[27] pyrrolyl arylsulfones (PASs),^[28–30] and indolyl aryl sulfones (IASs)^[31–33] as potent anti-HIV-1 agents (Figure 3) targeted against RT led us to design TIBO- and TBO-like sulfone derivatives represented by the general structures 1 and 2, respectively (Figure 4, Table 1).^[34,35] In particular, we recently reported the synthesis of 2,3-dihydroimidazo[1,5,4-ef][1,2,5]benzothiadiazepin-6(4*H*,7*H*)-one and -thione 1,1-dioxide (derivatives 1 **a–g**) as a new TIBO-related heterocyclic system.^[34] Compounds 1 (Figure 4a) are characterized by a sulfone group in place of the methylene group in position 6 of the TIBO ring, and are expected to have

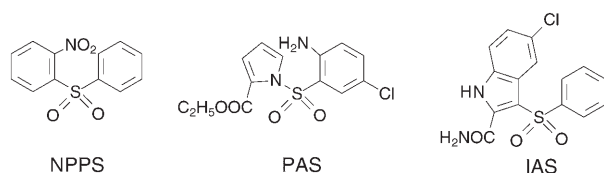


Figure 3. Sulfone derivatives active as anti-HIV-1 agents that target RT.

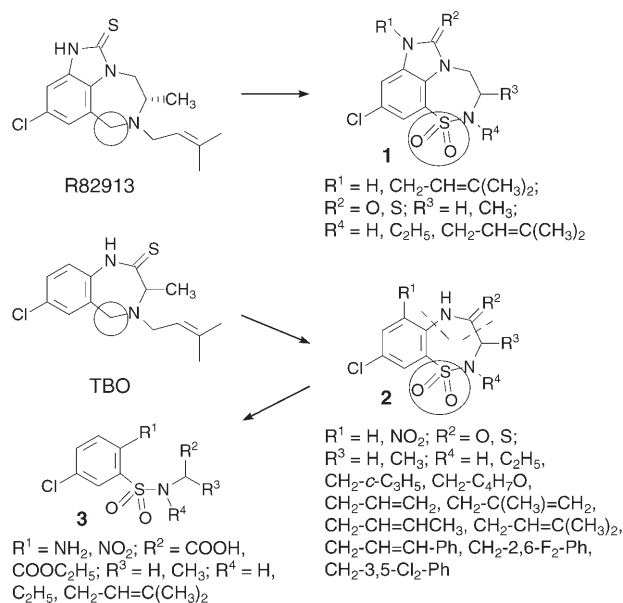
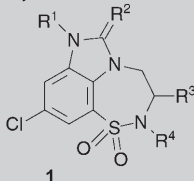
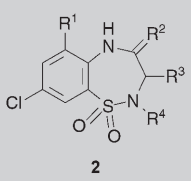
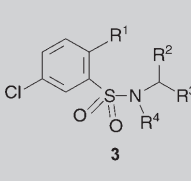
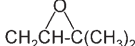
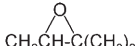


Figure 4. Planned modifications to a) TIBO and b) TBO structures for the newly designed anti-HIV-1 agents 1–3.

antiviral activity, as they are structurally related to R82913. This hypothesis was further supported by our previous studies on cyclic sulfones as HIV-1 RT inhibitors. In fact, derivatives 2 **c,m**, which were synthesized as part of a study on bi- and tricyclic benzothiadiazepinone congeners, showed promising anti-HIV-1 activity.^[35] Therefore, a number of 2-substituted benzothiadiazepines 2 (Figure 4b) were designed and synthesized as TBO sulfone analogues. The 3,3-dimethylallyl chain of R82913 and 2 **m** was replaced by various moieties with different stereochemical and/or electronic properties with the aim of enhancing the interaction between the newly designed inhibitors and RT. Moreover, both thiadiazepinone and -thione derivatives were tested for their activities against HIV-1. The acyclic precursors 3 (Figure 4b), used as intermediates in the synthesis of the cyclic derivatives, represent the ring-open counterparts of compounds 2, and were also evaluated as potential anti-HIV-1 agents. These compounds were expected to display some antiviral activity, as they are structurally related to NPPs, PASs, and IASs.

Herein, we describe the synthesis of the new derivatives 1 **h,i**, 2 **a,b,e–l,n–aa,ac**, and 3 **b,c,k**. We also present the cytotoxicity and anti-HIV-1 activities of all compounds 1–3. A X-ray crystallographic analysis was carried out to establish the absolute configuration of the enantiomers 2 **w** and 2 **x**, which were obtained by semipreparative HPLC of one of the most potent racemates, 2 **v**. Moreover, structural and molecular modeling studies were performed to elucidate the binding modes of 1–3 in the non-nucleoside binding site (NNBS) of HIV-1 RT. In particular, our aim was to develop a 3D QSAR model to rationalize the biological results and to predict the activity of novel untested TIBO- and TBO-like derivatives. To generate molecular descriptors, the GOLPE program^[36] for the multivariate regression analyses and the GRID program^[37] were used.

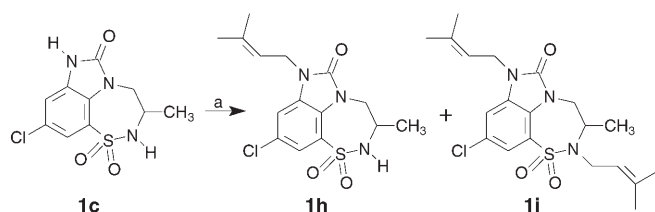
Table 1. Cytotoxicity, anti-HIV-1, and anti-rRT activities of TIBO- and TBO-like derivatives **1–3**.^[a]

<div style="display: flex; justify-content: space-around; align-items: center;"> <div style="text-align: center;">  <p>1</p> </div> <div style="text-align: center;">  <p>2</p> </div> <div style="text-align: center;">  <p>3</p> </div> </div>								
Compd	R ¹	R ²	R ³	R ⁴	CC ₅₀ ^[b]	EC ₅₀ ^[c]	SI ^[d]	IC ₅₀ ^[e]
1a	H	O	H	CH ₂ CH ₃	> 200	> 200	–	–
1b	H	S	H	CH ₂ CH ₃	> 200	127	1.6	–
1c	H	O	CH ₃	H	> 200	> 200	–	–
1d	H	O	CH ₃	CH ₂ CH ₃	130	> 130	–	–
1e	H	S	CH ₃	CH ₂ CH ₃	93	46	2	–
1f	H	O	CH ₃	CH ₂ CH=C(CH ₃) ₂	> 200	100	> 2	–
1g	H	S	CH ₃	CH ₂ CH=C(CH ₃) ₂	23	> 23	–	–
1h	CH ₂ CH=C(CH ₃) ₂	O	CH ₃	H	91	> 91	–	–
1i	CH ₂ CH=C(CH ₃) ₂	O	CH ₃	CH ₂ CH=C(CH ₃) ₂	63	> 63	–	–
2a	H	O	H	H	≥ 200	> 200	–	–
2b	NO ₂	O	H	H	> 200	> 200	–	–
2c	H	O	H	CH ₂ CH ₃	> 200	36	> 5.5	–
2d	NO ₂	O	H	CH ₂ CH ₃	> 200	> 200	–	–
2e	H	O	CH ₃	CH ₂ -c-C ₃ H ₅	> 200	2.2	> 91	–
2f	H	S	CH ₃	CH ₂ -c-C ₃ H ₅	> 200	10	> 20	–
2g	H	O	CH ₃	CH ₂ CH=CH ₂	> 200	28	> 7.1	–
2h	H	S	CH ₃	CH ₂ CH=CH ₂	16	> 16	–	–
2i	H	O	CH ₃	CH ₂ C(CH ₃)=CH ₂	≥ 200	17	≥ 11.8	–
2j	H	S	CH ₃	CH ₂ C(CH ₃)=CH ₂	47	> 47	–	–
2k	H	O	CH ₃	CH ₂ CH=CHCH ₃	> 200	0.7	286	–
2l	H	S	CH ₃	CH ₂ CH=CHCH ₃	57	1.4	41	–
2m	H	O	CH ₃	CH ₂ CH=C(CH ₃) ₂	> 200	0.8	> 250	0.94
2n	H	S	CH ₃	CH ₂ CH=C(CH ₃) ₂	> 200	4.6	> 43	–
2o	H	O	CH ₃		57	5	11	–
2p	H	O	CH ₃	CH ₂ CH=CHC ₆ H ₅	> 200	10	> 20	–
2q	H	S	CH ₃	CH ₂ CH=CHC ₆ H ₅	16	> 16	–	–
2r	H	O	CH ₃	CH ₂ (2-Me-C ₆ H ₄)	> 200	1	> 200	3.91
2s	H	S	CH ₃	CH ₂ (2-Me-C ₆ H ₄)	≥ 200	> 200	–	–
2t	H	O	CH ₃	CH ₂ (3-Me-C ₆ H ₄)	> 200	0.13	> 1538	1
2u	H	O	CH ₃	CH ₂ (3,5-(Me) ₂ -C ₆ H ₃)	> 200	0.12	> 1667	0.69
2v	H	O	CH ₃	CH ₂ (2,6-F ₂ -C ₆ H ₃)	> 200	0.2	> 1000	0.25
2w	H	O	S-CH ₃	CH ₂ (2,6-F ₂ -C ₆ H ₃)	> 200	0.07	> 2857	0.26
2x	H	O	R-CH ₃	CH ₂ (2,6-F ₂ -C ₆ H ₃)	> 200	0.2	> 1000	7.4
2y	H	S	CH ₃	CH ₂ (2,6-F ₂ -C ₆ H ₃)	≥ 200	9	≥ 22.2	–
2z	H	O	CH ₃	CH ₂ (3,5-Cl ₂ -C ₆ H ₃)	> 200	1.5	> 133	2.13
2aa	H	S	CH ₃	CH ₂ (3,5-Cl ₂ -C ₆ H ₃)	90	10	9	–
2ab	NO ₂	O	CH ₃	CH ₂ CH ₃	105	> 105	–	–
2ac	NO ₂	O	CH ₃		> 200	> 200	–	–
3a	NO ₂	COOCH ₂ CH ₃	H	H	73	> 73	–	–
3b	NH ₂	COOCH ₂ CH ₃	H	H	> 200	> 200	–	–
3c	NH ₂	COOH	H	H	> 200	> 200	–	–
3d	NO ₂	COOCH ₂ CH ₃	H	CH ₂ CH ₃	> 200	> 200	–	–
3e	NH ₂	COOCH ₂ CH ₃	H	CH ₂ CH ₃	> 200	> 200	–	–
3f	NH ₂	COOH	H	CH ₂ CH ₃	> 200	> 200	–	–
3g	NO ₂	COOCH ₂ CH ₃	CH ₃	CH ₂ CH ₃	105	> 105	–	–
3h	NH ₂	COOCH ₂ CH ₃	CH ₃	CH ₂ CH ₃	> 200	> 200	–	–
3i	NH ₂	COOH	CH ₃	CH ₂ CH ₃	> 200	> 200	–	–
3j	NO ₂	COOCH ₂ CH ₃	CH ₃	CH ₂ CH=C(CH ₃) ₂	91	> 91	–	–
3k	NO ₂	COOH	CH ₃	CH ₂ CH=C(CH ₃) ₂	≥ 200	> 200	–	–
3l	NH ₂	COOCH ₂ CH ₃	CH ₃	CH ₂ CH=C(CH ₃) ₂	> 200	2	> 100	–
3m	NH ₂	COOH	CH ₃	CH ₂ CH=C(CH ₃) ₂	> 200	109	> 1.8	–
R82913					30	0.03	1000	–
nevirapine					> 200	0.25	> 800	–

[a] Data represent mean values for three separate experiments; variation among triplicate samples was less than 15%. [b] compound concentration (μM) required to decrease the viability of mock-infected cells by 50% (MTT method). [c] compound concentration (μM) required for 50% protection of MT-4 cells from HIV-1-induced cytopathicity (MTT method). [d] selectivity index: CC₅₀/EC₅₀ ratio. [e] compound concentration (μM) required to inhibit the activity of HIV-1 rRT by 50%.

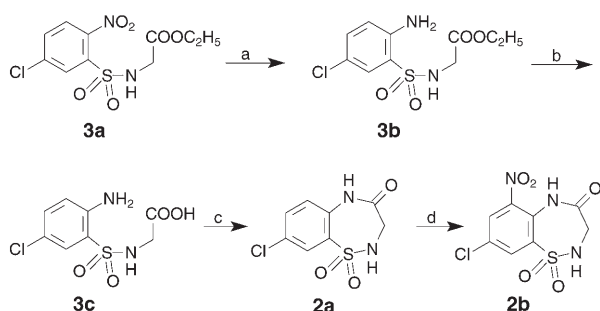
Chemistry

Compounds **1a–g**, **2c,d,m,ab**, and **3a,d–j,l,m** were obtained as reported previously,^[34,35] whereas the novel derivatives **1h,i**, **2a,b,e–l,n–aa,ac**, and **3b,c,k** were synthesized as shown in Schemes 1–4. In particular, the alkylation of **1c** with dimethyl-



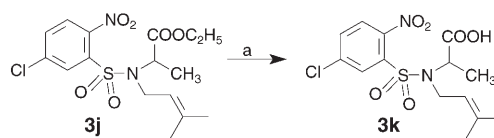
Scheme 1. Synthesis of compounds **1h** and **1i**: a) dimethylallyl bromide, K_2CO_3 , DMF, RT, 15 h.

allyl bromide in alkaline medium (K_2CO_3) at room temperature gave both **1h** and the corresponding bis-alkyl derivative **1i**, which were separated by chromatography (Scheme 1). Benzo-thiadiazepine **2a** and **2b** were accessed as shown in Scheme 2. Reduction of **3a**^[34] by heating with iron powder in



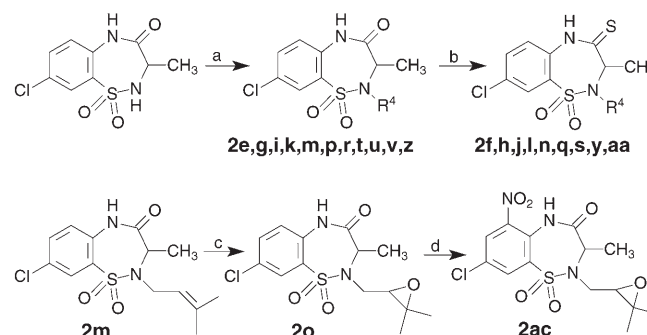
Scheme 2. Synthesis of compounds **3b,c** and **2a,b**: a) Fe, AcOH, 60 °C, 15 min; b) NaOH (1 N), THF/EtOH, RT, 2 h; c) EDCI, DMAP, THF, RT, 15 h; d) concentrated HNO_3 , 0 °C, 4 h.

glacial acetic acid at 60 °C gave the amino derivative **3b**, which was then hydrolyzed by NaOH (1 N) to afford **3c**. This compound was cyclized by treatment with the *N*-(3-dimethylaminopropyl)-*N'*-ethylcarbodiimide hydrochloride–dimethylamino pyridine (EDCI–DMAP) system to obtain derivative **2a**, which was then treated with concentrated HNO_3 at 0 °C to furnish **2b**. Hydrolysis of **3j** in alkaline medium (NaOH, 1 N) furnished the corresponding acid **3k** (Scheme 3), while alkylation of 8-chloro-2,3-dihydro-3-methyl-1,2,5-benzothiadiazepin-4(5*H*)-one 1,1-dioxide^[35] in the presence of K_2CO_3 at room temperature afforded derivatives **2e,g,i,k,m,p,r,t,u,v,z**, which were treated with Lawesson's reagent to give the corresponding thiones **2f,h,j,l,n,q,s,y,aa**. Finally, treatment of **2m**^[35] with *meta*-chloro-



Scheme 3. Synthesis of compound **3k**: a) NaOH (1 N), THF/EtOH, RT, 15 h.

perbenzoic acid (*m*-CPBA) led to **2o**, which was nitrated with concentrated HNO_3 to afford **2ac** (Scheme 4).



Scheme 4. Synthesis of compounds **2e–aa,ac**: a) alkyl halide, K_2CO_3 , DMF, RE; b) Lawesson's reagent, xylene, 100 °C; c) *m*-CPBA, $CHCl_3$, RT, 15 h; d) concentrated HNO_3 , –10 °C, 1 h.

Because of the well-known stereoselectivity of enantiomeric chiral TIBO derivatives,^[16–18] we decided to resolve one of the most potent racemates **2v** to determine the impact of chirality on the biological efficacy of this novel class of NNRTIs. Single enantiomers **2w** and **2x** were obtained by semipreparative HPLC of the racemic mixture on a polysaccharide-based chiral stationary phase (CSP)^[38] (Chiralpak AD), as reported previously.^[39] Furthermore, the absolute configuration of **2w** and **2x** was established by X-ray crystallographic analysis.

X-ray crystallography of (*R*)-**2x** and (*S*)-**2w**

As shown in Figure 5, the crystal structure of (*R*)-**2x** shows six independent molecules in the asymmetric unit. Each inde-

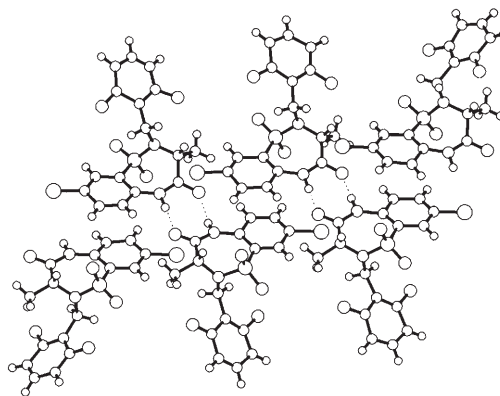


Figure 5. X-ray crystal structure of the *R* enantiomer **2x**: hydrogen bonds are shown by dashed lines.

pendent molecule has two chiral centers: the carbon atom carrying the methyl group, and the nitrogen atom carrying the difluorobenzyl group. The sum of the valence angles at the nitrogen atom varies from 351.6 to 357.1°, showing small pyramidalization. It is interesting to note that whereas the asymmetric carbon maintains the same configuration in the six independent molecules (*R*), the pyramidal nitrogen has an inverted configuration. As a consequence, its chirality is inverted in three of the molecules. The SO₂ oxygen atoms thus point in the opposite direction of the benzyl chain: on the same side of the hydrogen atom of the asymmetric carbon for the three lower molecules, and on the other side for the three upper molecules. In Figure 5 the lower three molecules have opposite configurations about the nitrogen atoms from those of the upper molecules. The change of nitrogen chirality is only evidenced in the solid state; this phenomenon does not appear in solution as a result of the rapid interconversion between the two forms.

The three lower molecules share roughly the same conformation, particularly that of the seven-membered ring, as the group of the three upper molecules. The two groups have different nitrogen atom chirality, and different conformations of the seven-membered ring. The lower three molecules have six coplanar atoms, the pyramidal nitrogen atom has an average distance of 0.77 Å from this plane, and the average amidic bond angle is −7.2°; the three upper molecules have five coplanar atoms, the pyramidal nitrogen atom and the asymmetric carbon atom have an average distance of 1.13 and 0.82 Å from the same side of the plane, respectively, and the average amidic bond angle is 16.2°.

All the N–H and C=O groups are involved in hydrogen bonds (N...O distance: 2.90 Å (average), 2.86 Å (minimum), 2.93 Å (maximum)) to form dimers between two molecules with different nitrogen atom chirality (Figure 5). The packing of the dimers is mainly governed by van der Waals forces and π – π stacking interactions between aromatic ring pairs (distances between the centers of the aromatic rings: 3.75, 3.73, and 3.77 Å).

Figure 6 shows the crystal structure of (*S*)-**2w**, which presents two independent molecules in the asymmetric unit. As is

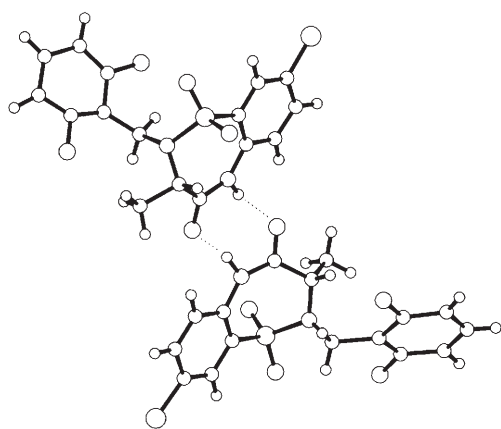


Figure 6. X-ray crystal structure of the *S* enantiomer **2w**: hydrogen bonds are shown by dashed lines.

the case for the *R* enantiomer, every independent molecule has the same two chiral centers. The sums of the valence angles at the pyramidal nitrogen atoms are 349.8 and 352.2°. In this case, the asymmetric carbon atom also maintains the same configuration in the two independent molecules and the pyramidal nitrogen atom inverts its configuration to bring the SO₂ oxygen atoms to point in the opposite direction of the benzyl chain. In Figure 6, the lower molecule has *S* and *R* configurations for the carbon and nitrogen atoms, respectively, whereas the upper molecule has *S* and *S* configurations.

Also in this case, the conformation of the seven-membered ring differs between the two molecules: the *S,S* molecule has six coplanar atoms, the pyramidal nitrogen atom has a distance of 0.85 Å from the root mean square plane and the amidic bond angle is −3.5°. The *S,R* molecule has five coplanar atoms, the asymmetric carbon atom and the pyramidal nitrogen atom are separated from the same side of the root mean square plane by 0.82 and 1.18 Å, respectively, and the amidic bond angle is −19.9°.

The N–H and C=O groups of two molecules with different configuration about the nitrogen atom are involved in two hydrogen bonds (N...O distances of 2.94 and 2.83 Å) that form a dimer (Figure 6). The packing of the dimers is mainly governed by van der Waals forces and by π – π stacking interactions between aromatic ring pairs (distance between the centers of the aromatic rings: 3.83 Å).

Results and Discussion

Anti-HIV-1 cell-based assays and anti-rRT assays

The novel TIBO- and TBO-like derivatives **1–3** were evaluated for their cytotoxicity and anti-HIV-1 activity in MT-4 cells, with nevirapine^[7] and the TIBO derivative R82913^[12] as reference drugs. The results, expressed as CC₅₀ (cytotoxicity), EC₅₀ (anti-HIV-1 activity) and SI (selectivity index, given by the CC₅₀/EC₅₀ ratio) values, are summarized in Table 1. Of the 51 derivatives tested, 25 were active in the concentration range of 0.07–127 μ M. Within the group of acyclic sulfonamides **3**, only derivatives **3l** and **3m** were moderately active. Surprisingly, similar results were observed for imidazobenzothiadiazepinone derivatives **1**. In fact, derivatives **1b,e,f** were active at concentrations ranging from 46 to 100 μ M, whereas the remaining compounds were inactive at subcytotoxic concentrations, including **1g**, the sulfone analogue of R82913. On the other hand, good results were found within the benzothiadiazepine series (compounds **2**). In fact, 20 out of 29 derivatives **2** were active in the concentration range of 0.07–36 μ M. Consequently, further SARs are discussed only on derivatives **2**. Contrary to our expectations, the thiones were less active than the corresponding carbonyl derivatives (compare **2f,h,j,l,n,q,s,y,aa** with respective compounds **2e,g,i,k,m,p,r,v,z**) which represents a reversal of the trend observed within the TIBO series. Interestingly, the presence of a C–C double bond at the 2 position in the alkyl chain and a methyl group in the 3 position of the benzothiadiazepine ring enhanced the activity of **2a** (*R*⁴=H) and **2c** (*R*⁴=C₂H₅), as expected from previous results.^[35] On the other

hand, the introduction of a nitro group on the phenyl ring led to inactive derivatives **2b,d**. The best results were obtained with compounds in which the alkyl or alkenyl chain was replaced with a benzyl moiety (derivatives **2r,t-v,z**). Among the substituted benzyl derivatives, compounds **2t** (3-methylated), **2u** (3,5-dimethylated), and **2v** (2,6-difluorinated) were the most potent racemates of the series, with potencies in the sub-micromolar range ($EC_{50} = 0.12\text{--}0.2\ \mu\text{M}$). Separation of racemate **2v** led to the *R* and *S* enantiomers **2x** and **2w**, respectively. Biological assays showed that the *S* isomer **2w** was threefold more potent than the *R* counterpart **2x**. This result emphasizes the vital role played by the C3 stereogenic center in obtaining the highest anti-HIV-1 activity within this novel series of NNRTIs, and is in agreement with SARs found for TIBO derivatives.^[16–18] The most potent compound **2w** had an EC_{50} value of $0.07\ \mu\text{M}$, and was three to fourfold more potent than nevirapine and twofold less potent than R82913. However, the SI of **2w** (>2857) was higher than those of R82913 ($SI = 1000$) and nevirapine ($SI > 800$).

To determine whether the title compounds target HIV-1 RT, representative derivatives (**2m,r,t-x,z**) were assayed against the recombinant enzyme (rRT). All compounds inhibited the viral enzyme at concentrations similar to those active in cell-based assays. These results, expressed as IC_{50} values in Table 1, suggest that compounds **1–3** targeted HIV-1 RT. Furthermore, compounds **2m,w** were tested against clinically relevant, drug-resistant RT forms carrying K103N and Y181I mutations. Unfortunately, neither **2m** nor **2w** were active at concentrations below $50\ \mu\text{M}$ (data not shown). A molecular modeling study was therefore undertaken to rationalize the surprising results obtained for derivatives **1–3**.

GRID/GOLPE 3D QSAR and docking of TIBO- and TBO-like sulfone derivatives 1–3.

Training set: A training set of all the TIBO- and TBO-like sulfone derivatives **1–3** reported in Table 1 (51 compounds) was used to develop the 3D QSAR model. Since the *S* enantiomer **2w** was found to be more active than the *R* isomer **2x**, the structures of the training set were modeled starting from the coordinates of the above-described crystal structure with the MAESTRO program.^[40]

Alignment rules: Receptor-based alignment rules^[41,42] were obtained by means of molecular mechanics and docking experiments on the training set into the NNBS extracted from the crystal structure of R82913–RT complex (PDB entry code: 1tvr).^[43] In several cases, different binding modes were found among the conformations suggested by the AutoDock program.^[44]

As the molecular alignment of the training set is a crucial step in a 3D QSAR, four different alignment rules were used: 1) the ligand conformations extracted from the corresponding minimized complex with RT (termed Min alignment), 2) the ligand conformations extracted from the preceding minimized complex after a molecular dynamics (MD) run (termed Dyn alignment), 3) the first-ranked docked conformations as obtained from the AutoDock run (termed Best Docked align-

ment), and 4) the lowest-energy docked conformations of the most populated clusters (termed Best Cluster alignment).

Calculation of molecular interaction fields (MIFs): The MIFs for the 3D QSAR studies were calculated with the GRID program.^[37,45] The NNBS is characterized by at least two important spatial regions: 1) the hydrophobic aromatic-rich binding pocket formed primarily by residues Tyr181, Tyr188, Phe227, and Trp229; and 2) the hydrogen-bonding site, where most of the known RT inhibitors make at least one hydrogen bond with either the amide or carbonyl group of Lys101. To include these two binding-site features into the 3D QSAR studies, the aromatic carbon probe (grid format C1 =) and the water probe (grid format OH2) were used to calculate the MIFs.

Definition of the 3D QSAR models: The program GOLPE45^[45,46] was used to define eight 3D QSAR models obtained from the combinations of four alignments (Min, Dyn, Best Cluster and Best Docked) and two MIFs (aromatic or water) (Table 2). The MIFs of the training set were imported

Table 2. Statistical results of the 3D QSAR models.

Model	Alignment	GRID probes	Number of variables	r^2_{max}	q^2_{max}	SDEP _{CV}	PC ^[a]
1	Min	OH2	1060	0.84	0.68	0.62	3
2	Min	C1 =	1037	0.75	0.59	0.70	2
3	Dyn	OH2	936	0.91	0.71	0.58	3
4	Dyn	C1 =	1142	0.85	0.67	0.62	3
5	Best Docked	OH2	944	0.92	0.72	0.55	3
6	Best Docked	C1 =	867	0.93	0.72	0.54	3
7	Best Cluster	OH2	977	0.92	0.80	0.48	3
8	Best Cluster	C1 =	1060	0.91	0.83	0.46	3

[a] Number of principal components that showed the maximum q^2 value.

into GOLPE along with the inverse logarithm of the experimental anti-HIV-1 activities (pEC_{50} values). It could be argued that cell-based activities are not suitable for such 3D QSAR studies; enzyme-based assays (IC_{50} values) are a more appropriate choice. Nevertheless, it has been proven that for TIBO derivatives, there is a good correlation between enzyme-based (IC_{50}) and cell-based (EC_{50}) assays.^[24] Therefore, data derived from cell-based activities were not expected to affect the 3D QSAR. Moreover, we aimed to obtain a 3D QSAR model capable of discriminating between active and inactive derivatives, with the latter group as a source of important structural information. Inactive compounds were thus included in the training set, to which an EC_{50} value equal to 50% that of the least-active compound was arbitrarily assigned^[47,48] (Table 1).

After data pre-treatment (Experimental Section), consecutive fractional factorial design (FFD) selections were conducted to refine the initial models. The FFD selections were continued until no further statistical improvements were observed. From the initial 17457 grid variables, the data pre-treatment and FFD selections led to final models that contained only ≈ 1000 descriptive variables (Table 2). To measure the goodness of the models, the statistical indices r^2 (correlation coefficient), q^2 (predictive correlation coefficient) and SDEP_{CV} (cross-validated

standard deviation error of prediction) were used. The eight final 3D QSAR models were characterized by r^2 , q^2 , and $SDEP_{CV}$ values falling in the ranges 0.75–0.93, 0.59–0.83, and 0.46–0.70, respectively (Table 2). For both the FFD selections and the cross-validations, the group method was used, in which the number of groups to be used was set to five.

Based on the statistical indices (r^2 , q^2 , and $SDEP_{CV}$), the Best Cluster alignment shown in Figure 7 proved to be the most

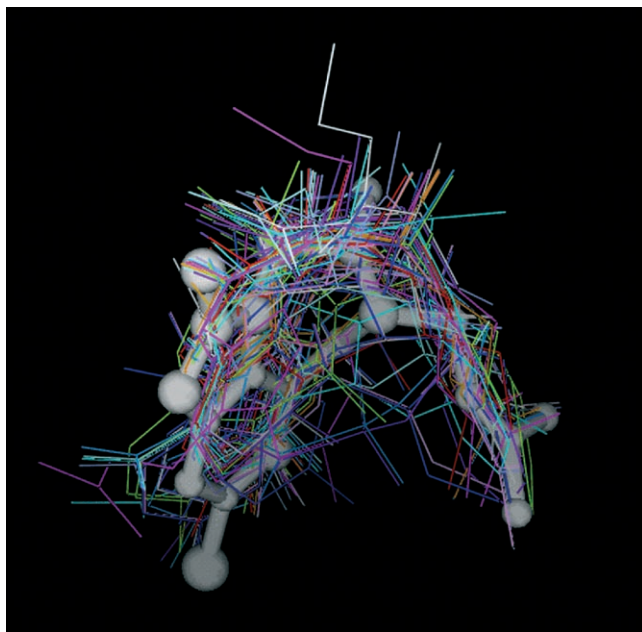


Figure 7. Best Cluster alignment of the training set molecules as obtained from AutoDock.

robust and self-consistent model. Therefore, models 7 and 8 reported in Table 2 were chosen for the description of the 3D QSAR maps, and only their interpretation was given. Attempts to merge the two models into one that contains both the C1= and OH2 MIFs did not afford a better model (data not shown).

Interpretation of models 7 and 8: One important feature of 3D QSAR is the graphical representation of the model, which makes its interpretation easier. In the GOLPE software, several options are available to display the final model. Among these, the partial least squares (PLS) pseudo-coefficients and the activity contribution plots are very useful. The PLS pseudo-coefficients plot allows visualization of the selected grid points at determined energy levels of a given molecule–probe interaction to provide graphical information of the whole training set. However, in this plot, the signs of the coefficients can induce errors, as coefficients carry opposite meaning that depends on whether the compound produces positive or negative field values in a specific area. The PLS coefficients plots of the highly active compound **2w** ($EC_{50}=0.07\text{ }\mu\text{M}$) and the weak compound **1f** ($EC_{50}=100\text{ }\mu\text{M}$) are reported in Figure 8. Models 7 and 8 were used, which reflect the overall graphical

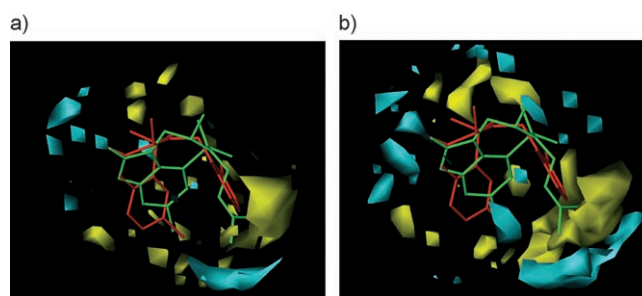


Figure 8. GRID/GOLPE PLS coefficient contour maps for the 3D QSAR models a) 7 and b) 8. Polyhedrons in yellow are positive coefficients (data level = +0.0050) and polyhedrons in cyan are negative coefficients (data level = −0.0050). To aid interpretation, the highly active compound **2w** is displayed in red and the weakly active compound **1f** in green. Hydrogen atoms have been omitted for clarity.

representation of the 3D QSAR models for the 51 compounds in the training set.

Negative PLS coefficients, individualized in the cyan polyhedrons, indicate regions where favorable interactions lead to increased activity. On the contrary, yellow polyhedrons (positive PLS coefficients) represent regions where unfavorable interactions lead to decreased activity.

By comparing the PLS coefficient plots obtained from model 7 (water probe) and 8 (aromatic probe), it can be observed that the two models give similar information. This is may be due to the fact that the structural variance is related more to the hydrophobic nature of the molecules than to their electrostatic characteristics; thus the hydrogen-bonding information provided by the water probes is less influential. This is in perfect agreement with the NNBS environment, which is constituted mainly by hydrophobic side chains. As can be observed in Figure 8, either yellow or cyan polyhedrons surround primarily the dimethylallyl (**1f**) and difluorobenzyl (**2w**) moieties in both C1= and OH2 GRID fields, which suggests that these regions are the most responsible for the differences in activities throughout the molecular series. Of particular interest is the C1= PLS coefficient plot (Figure 8b), in which the wider yellow polyhedron closer to the structures with respect to the cyan polyhedron indicates that an aromatic/hydrophobic portion (a dimethylallyl or difluorobenzyl group) leads to favorable interactions (cyan polyhedron). At the same time, however, these groups are not allowed to overcome a well-defined space indicated by the large yellow polyhedrons, where unfavorable interactions occur. Smaller cyan polyhedrons are situated in proximity to the carbonyl groups of either **1f** or **2w**, which indicates the presence of a favorable interaction, probably through a hydrogen bond. On the other hand, smaller yellow polyhedrons in the top and bottom regions of Figure 8 indicate areas where increased steric hindrance could lead to a decrease in activity.

Whereas the PLS coefficient plots give a global interpretation of the 3D QSAR model, the activity contribution plot displays spatial regions that are individually important for the selected molecule. The activity contribution plot, which differs for every molecule of the training set, results from multiplica-

tion of the values of the coefficients by the actual values of the field for the molecule in question. The activity contribution plots of the highly active compound **2w** and the weak compound **1f** are shown in Figure 9.

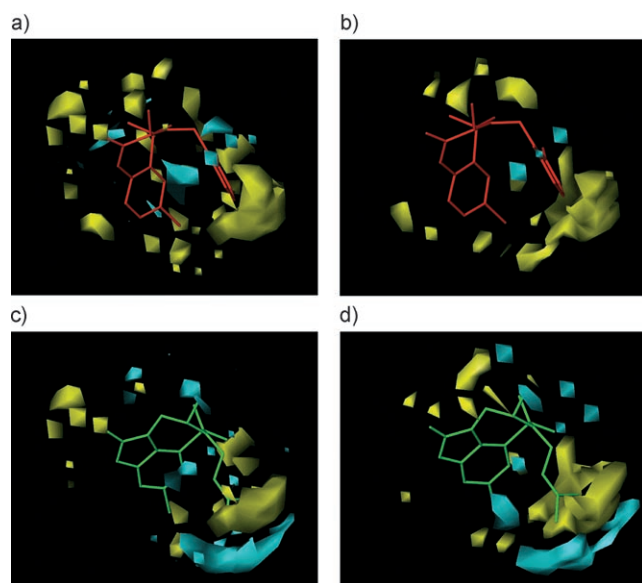


Figure 9. Activity contribution plots of the representative highly active compound **2w** (red) and of the representative weakly active compound **1f** (green): a,c) plots related to model 7; b,d) plots for the model 8. Positive contribution to the activity is color-coded as yellow polyhedra and negative contribution to the activity is color-coded as cyan polyhedra.

In the activity contribution plots, cyan polyhedrons indicate regions in which a negative contribution to the inhibitory activity is associated, whereas yellow polyhedrons show areas of positive contribution to the anti-HIV activity. Interestingly, the scaffold (Table 1) of compounds **2** allows the difluorobenzyl moiety of **2w** to make only favorable interactions (Figure 9a,b). On the contrary, the larger and more rigid tricyclic scaffold of compounds **1** pushes the dimethylallyl group of **1f** toward the yellow cloud of the PLS coefficients plots (Figure 8) and generates the cyan polyhedrons (Figure 9c,d) as a measure of the decreased anti-HIV activity. The presence of yellow polyhedrons near the carbonyl moiety in both the active (**2w**) and weakly active (**1f**) compounds (Figure 9a,c, OH2 probe) indicates that the scaffold of compound **1f** is responsible for the decreased anti-HIV activity, mainly as a result of steric hindrance exerted by the N substituents.

As a rule, the 3D QSAR maps cannot be employed to extract information about ligand–receptor interactions, as the model has been created only with the structures included in the training set. This implies that the reliability of any receptor model can be severely limited by the quality of the design procedure and of the correlation between structural features and alignments. However, as the alignment of the compound training set was based on molecular docking, it is useful to check for matches between the receptor pocket (NNBS) and the 3D QSAR maps. Figure 10 shows a 4-Å core of NNBS residues containing **2w** and **1f**. The core is overlapped with the 3D PLS co-

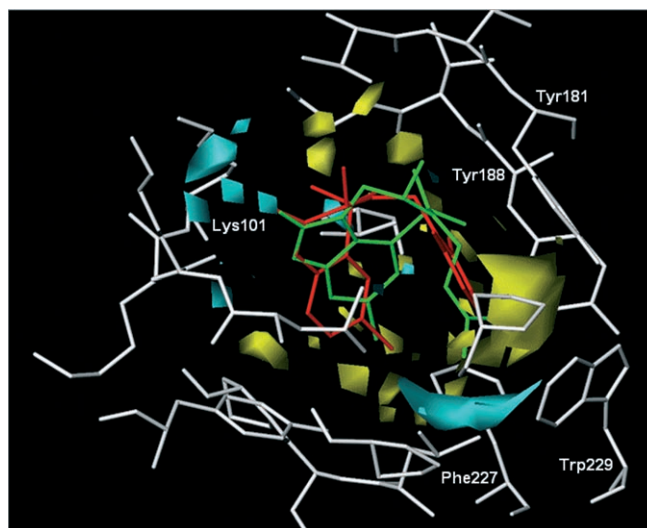


Figure 10. PLS coefficient maps of model 7 superimposed on a 4-Å core of NNBS. Derivatives **2w** (red) and **1f** (green) are also displayed. Only the residues relevant to the discussion in the text are shown for clarity.

efficients maps of model 7; the close match between the NNBS residues and the PLS polyhedrons is evident. In particular, the large cyan and yellow polyhedrons (Figure 10, lower right) fit exactly in the hydrophobic aromatic-rich pocket formed mainly by the side chains of Tyr181, Tyr188, Phe227, and Trp229, whereas the smaller cyan polyhedrons overlap the hydrogen bond that can be established between the N–H group of Lys101 and the carbonyl group of either **2w** or **1f**.

Binding-mode analysis of TIBO- and TBO-like sulfones 1–3: Receptor-based alignment aside, the docking of **1–3** into the NNBS could give further insight on the binding mode of this new class of compounds. Differences in binding mode were observed as a function of the molecular scaffold used (compounds **1**, **2**, or **3**). Superimpositions of the most active derivative for each of the three scaffolds **1e**, **2w**, and **3l** with the bound conformation of the reference drug R82913 are shown in Figure 11. Because of the best 3D QSAR models 7

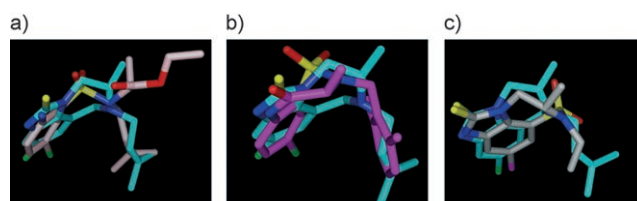


Figure 11. Superimposition of the bound conformation of R82913 (cyan) with the docking results on derivatives a) **3l** (colored by atom), b) **2w** (magenta), and c) **1e** (colored by atom).

and 8 (discussed above), the Best Cluster alignment was selected for the binding-mode comparison. Derivative **3l** appears to maintain the overall binding mode of R82913, with an almost complete overlap of the shared chlorophenyl and dimethylallyl substructures. However, as the molecule is in the open form,

the ethyloxycarbonyl moiety generates some negative interactions in the NNBS which could explain the moderate activity of **3l** itself. The binding mode of **2w** resembles that of **3l** and shares the best feature overlap with R82913, which explains its status as the most active derivative of the whole series. The binding mode of **1e** is also interesting. Among the three compounds examined, **1e** is structurally closer to R82913, although it appears that the SO₂ group introduces differences sufficient to drive the molecule to rearrange its binding conformation. As a result, the chiral methyl substituent is shifted to a different region, and its role is replaced by the SO₂ group.

Conclusions

TIBO- and TBO-like sulfones **1–3** were designed and synthesized as a new class of NNRTI. These compounds showed interesting activities against the HIV-1 replication cycle in cell-based assays and were shown to target RT in enzyme assays. Compound **2w** showed anti-HIV-1 activity (EC₅₀=0.07 μ M, CC₅₀>200 μ M, SI>2857) similar to that of TIBO derivative R82913 (EC₅₀=0.03 μ M, CC₅₀=30 μ M, SI=1000), used as a reference drug. Unexpectedly, the biological activities of the title compounds **1–3** did not parallel the results found for the TIBO class. In particular, compound **1g**, although closely related to the chemical structure of R82913, proved to be completely inactive. Better results were obtained with TBO-like sulfones **2**, which showed which were active at sub-micromolar concentrations in some cases. One of the most potent racemates (**2v**) was separated by semipreparative HPLC to give the single enantiomers **2w** and **2x**, whose absolute configuration was determined by X-ray diffraction studies. The results of these structural studies helped to better elucidate the geometry of the substituents around C3 of the benzothiadiazepine ring, and to conduct molecular modeling studies on derivatives **1–3**. Indeed, a receptor-based 3D QSAR model capable of rationalizing the biological results and predicting the activity of novel TIBO- and TBO-like derivatives was developed by using the programs AutoDock, GRID, and GOLPE, with a training set of 51 TIBO- and TBO-like derivatives. The derived 3D QSAR models showed conventional correlation (r^2) and cross-validated (q^2) coefficient values that ranged from 0.75 to 0.93 and from 0.59 to 0.83, respectively. Among the eight models developed, the most predictive models 7 and 8 were used to interpret the SARs of 51 TIBO- and TBO-like derivatives. Moreover, the docking results revealed that relative to R82913, the introduction of the SO₂ group leads to a different binding mode, which could explain the weaker anti-HIV activity of the SO₂-modified TIBO derivatives.

As none of the derivatives **1–3** were found to be active against clinically relevant mutant RT forms such as those with the K103N and Y181I point mutations, further studies are being carried out with the goal of generating potent TBO-like sulfones that are active against HIV-1 mutant strains resistant to the NNRTIs already on the market.

Experimental Section

Materials: Melting points were determined on a Büchi 530 melting point apparatus and are uncorrected. IR spectra (nujol mulls) were recorded on a Perkin–Elmer 297 spectrophotometer. ¹H NMR spectra were recorded at 200 MHz on a Bruker AC 200 spectrometer with Me₄Si as the internal reference standard. All compounds were routinely checked by TLC and ¹H NMR spectroscopy. TLC was performed by using aluminum-baked silica gel plates (Fluka DC-Alufolien Kieselgel 60 F₂₅₄). Developed plates were visualized with UV light. Solvents were reagent grade and, when necessary, were purified and dried by standard methods. A rotary evaporator (Büchi) operating under reduced pressure (\approx 20 Torr) was used to concentrate solutions after reactions and extractions. Organic solutions were dried over anhydrous sodium sulfate. Analytical results agreed to within \pm 0.40% of the theoretical values. All newly synthesized compounds were analyzed for C, H, N, S, Cl, and, when present, F.

Syntheses: General procedure for the preparation of compounds **1h,i** and **2e,g,i,k,p,r,t,u,v,z**; example: 8-chloro-2-[(3,5-dichlorophenyl)methyl]-2,3-dihydro-3-methyl-1,2,5-benzothiadiazepin-4(5H)-one 1,1-dioxide (**2z**). A suspension of 8-chloro-2,3-dihydro-3-methyl-1,2,5-benzothiadiazepin-4(5H)-one 1,1-dioxide^[35] (500 mg, 1.9 mmol), 3,5-dichlorobenzyl bromide (370 mg, 1.9 mmol), and K₂CO₃ (270 mg, 1.9 mmol) in anhydrous *N,N*-dimethylformamide (DMF) (3 mL) was stirred at room temperature for 15 h. Water was then added (20 mL), and the mixture was extracted with ethyl acetate (3 \times 10 mL). The organic extracts collected were washed with brine (3 \times 10 mL) and dried. Evaporation of the solvent gave crude product, which was separated by chromatography on a silica gel column to afford pure **2z** (370 mg, 46%); m.p. 253–254 °C (from benzene); IR $\tilde{\nu}$ =3190 (NH) and 1650 cm⁻¹ (CO); ¹H NMR ([D₆]DMSO): δ =1.35 (d, 3H, CH₃), 4.30 (s, 2H, CH₂), 4.70 (q, 1H, CH), 7.30–7.37 (m, 3H, benzene C3–H and benzyl C2–H, C6–H), 7.54 (m, 1H, benzene C4–H), 7.67–7.70 (m, 2H, benzene C6–H and benzyl C4–H), 10.50 ppm (br s, 1H, NH).

Halide used as reagent; yield; reaction time; chromatographic system; melting point; recrystallization solvent; IR spectroscopic data; and ¹H NMR spectroscopic data are listed for each of the following compounds:

1h: 3,3-dimethylallyl bromide; 28%; 15 h; SiO₂ (chloroform/ethyl acetate, 1:1); oil; IR: $\tilde{\nu}$ =3080 (NH) and 1670 cm⁻¹ (CO); ¹H NMR (CDCl₃): δ =1.43 (d, 3H, CHCH₃), 1.76 and 1.85 (2 s, 6H, =C–CH₃), 3.90–4.22 (m, 2H, CH–CH₃ and CHH), 4.40–4.70 (m, 3H, CH₂–C= and CHH), 5.07 (br s, 1H, NH), 5.21 (m, 1H, =CH), 7.00 and 7.42 ppm (2 d, J_m =2.0 Hz, 2H, benzene C8–H and C10–H).

1i: 3,3-dimethylallyl bromide; 18%; 15 h; SiO₂ (chloroform/ethyl acetate, 1:1); oil; IR: $\tilde{\nu}$ =1660 cm⁻¹ (CO); ¹H NMR (CDCl₃): δ =1.44 (d, 3H, CHCH₃), 1.50, 1.54, 1.75 and 1.85 (4 s, 12H, =C–CH₃), 3.74–3.83 (m, 3H, CH–CH₃ and CH₂), 4.47 (d, 4H, CH₂–C=), 4.85 and 5.21 (2 m, 2H, =CH), 6.99 and 7.40 ppm (2 d, J_m =2.0 Hz, 2H, benzene C8–H and C10–H).

2e: cyclopropylmethyl bromide; 75%; 48 h; SiO₂ (chloroform/ethyl acetate, 20:1); 190–192 °C; benzene; IR: $\tilde{\nu}$ =3190 (NH) and 1650 cm⁻¹ (CO); ¹H NMR (CDCl₃): δ =0.16–0.32 (m, 2H, CH₂), 0.40–0.51 (m, 2H, CH₂), 0.98 (m, 1H, CH), 1.28–1.75 (m, 3H, CH₃), 3.08 (d, 2H, N–CH₂), 4.64 (q, 1H, CH), 7.05 (d, J_o =8.6 Hz, 1H, benzene C3–H), 7.46 (dd, J_o =8.6 Hz, J_m =2.4 Hz, 1H, benzene C4–H), 7.90 (d, J_m =2.4 Hz, 1H, benzene C6–H), 8.87 ppm (br s, 1H, NH).

2g: allyl bromide; 56%; 72 h; SiO₂ (chloroform/ethyl acetate, 20:1); 211–212 °C; benzene; IR: $\tilde{\nu}$ =3190 (NH) and 1640 cm⁻¹ (CO); ¹H NMR (CDCl₃): δ =1.66 (d, 3H, CH₃), 3.80 (m, 2H, CH₂), 4.51 (q, 1H, CH), 5.26 (m, 2H, =CH₂), 5.75 (m, 1H, =CH), 7.06 (d, J_o =8.7 Hz, 1H, benzene C3–H), 7.47 (dd, J_o =8.7 Hz, J_m =2.4 Hz, 1H, benzene

C4–H), 7.92 (d, $J_m = 2.4$ Hz, 1 H, benzene C6–H), 8.83 ppm (br s, 1 H, NH).

2i: 3-chloro-2-methylpropene; 60%; 72 h; SiO₂ (chloroform/ethyl acetate, 20:1); 179–181 °C; benzene; IR: $\tilde{\nu} = 3190$ (NH) and 1650 cm⁻¹ (CO); ¹H NMR (CDCl₃): $\delta = 1.67$ (d, 3 H, CH₃), 1.80 (s, 3 H, =C–CH₃), 3.63 (s, 2 H, CH₂), 4.47 (q, 1 H, CH), 5.02 (s, 2 H, =CH₂), 7.15 (d, $J_o = 8.7$ Hz, 1 H, benzene C3–H), 7.48 (dd, $J_o = 8.7$ Hz, $J_m = 2.4$ Hz, 1 H, benzene C4–H), 7.89 (d, $J_m = 2.4$ Hz, 1 H, benzene C6–H), 9.50 ppm (br s, 1 H, NH).

2k: 1-bromo-2-butene; 56%; 96 h; SiO₂ (chloroform/ethyl acetate, 20:1); 153–155 °C; benzene; IR: $\tilde{\nu} = 3190$ (NH) and 1640 cm⁻¹ (CO); ¹H NMR (CDCl₃): $\delta = 1.66$ –1.69 (m, 6 H, CH₃), 3.75 (d, 2 H, CH₂), 4.45 (q, 1 H, CH), 5.31 and 5.75 (2 m, 2 H, =CH), 7.08 (d, $J_o = 8.7$ Hz, 1 H, benzene C3–H), 7.48 (dd, $J_o = 8.7$ Hz, $J_m = 2.1$ Hz, 1 H, benzene C4–H), 7.90 (d, $J_m = 2.1$ Hz, 1 H, benzene C6–H), 9.04 ppm (br s, 1 H, NH).

2p: cinnamyl bromide; 76%; 3.5 h; SiO₂ (chloroform/ethyl acetate, 5:1); 194–196 °C; benzene; IR: $\tilde{\nu} = 3190$ (NH) and 1650 cm⁻¹ (CO); ¹H NMR (CDCl₃): $\delta = 1.70$ (d, 3 H, CH₃), 4.00 (m, 2 H, CH₂), 4.55 (q, 1 H, CH), 6.10 (dd, $J_t = 15.8$ Hz, $J_o = 6.7$ Hz, 1 H, CH₂–CH=), 6.51 (d, $J_t = 15.8$ Hz, 1 H, =CH–Ar), 6.97 (d, $J_o = 8.6$ Hz, 1 H, benzene C3–H), 7.30–7.33 (m, 5 H, benzene C–H), 7.45 (dd, $J_o = 8.6$ Hz, $J_m = 2.4$ Hz, 1 H, benzene C4–H), 7.95 (d, $J_m = 2.4$ Hz, 1 H, benzene C6–H), 8.41 ppm (br s, 1 H, NH).

2r: 2-methylbenzyl chloride; 60%; 48 h; SiO₂ (chloroform/ethyl acetate, 20:1); 210–212 °C; ethanol; IR: $\tilde{\nu} = 3190$ (NH) and 1650 cm⁻¹ (CO); ¹H NMR (CDCl₃): $\delta = 1.44$ (d, 3 H, CH₃–CH), 2.37 (s, 3 H, CH₃), 4.13 (d, 1 H, CHH), 4.37–4.45 (m, 2 H, CH and CHH), 7.10 (d, $J_o = 8.6$ Hz, 1 H, benzene C3–H), 7.22–7.33 (m, 4 H, benzene C–H), 7.50 (dd, $J_o = 8.6$ Hz, $J_m = 2.4$ Hz, 1 H, benzene C4–H), 7.94 (d, $J_m = 2.4$ Hz, 1 H, benzene C6–H), 8.92 ppm (br s, 1 H, NH).

2t: 3-methylbenzyl bromide; 41%; 2.5 h; SiO₂ (chloroform/ethyl acetate, 20:1); 201–203 °C; ethanol; IR: $\tilde{\nu} = 3190$ (NH) and 1660 cm⁻¹ (CO); ¹H NMR ([D₆]DMSO): $\delta = 1.30$ (d, 3 H, CH₃–CH), 2.27 (s, 3 H, CH₃), 4.27 (s, 2 H, CH₂), 4.53 (q, 1 H, CH), 7.01–7.31 (m, 5 H, benzene C–H and benzyl C–H), 7.65–7.70 (m, 2 H, benzene C–H), 10.56 ppm (br s, 1 H, NH).

2u: 3,5-dimethylbenzyl bromide; 26%; 15 h; SiO₂ (chloroform/ethyl acetate, 20:1); 221–223 °C; benzene; IR: $\tilde{\nu} = 3190$ (NH) and 1660 cm⁻¹ (CO); ¹H NMR ([D₆]DMSO): $\delta = 1.32$ (d, 3 H, CH₃–CH), 2.33 (s, 6 H, CH₃), 4.31 (s, 2 H, CH₂), 4.55 (q, 1 H, CH), 7.05–7.33 (m, 4 H, benzene C–H and benzyl C–H), 7.68–7.72 (m, 2 H, benzene C–H), 10.57 ppm (br s, 1 H, NH).

2v: 2,6-difluorobenzyl bromide; 57%; 72 h; SiO₂ (chloroform/ethyl acetate, 20:1); 212–213 °C; benzene; IR: $\tilde{\nu} = 3190$ (NH) and 1640 cm⁻¹ (CO); ¹H NMR (CDCl₃): $\delta = 1.67$ (d, 3 H, CH₃), 4.43–4.57 (m, 3 H, CH and CH₂), 6.82–6.86 (m, 2 H, benzyl C3–H and C5–H), 6.97 (d, $J_o = 8.7$ Hz, 1 H, benzene C3–H), 7.30–7.37 (m, 1 H, benzyl C4–H), 7.39 (dd, $J_o = 8.7$ Hz, $J_m = 2.4$ Hz, 1 H, benzene C4–H), 7.76 (d, $J_m = 2.4$ Hz, 1 H, benzene C6–H), 8.90 ppm (br s, 1 H, NH).

2z: 3,5-dichlorobenzyl chloride; 46%; 15 h; SiO₂ (chloroform/ethyl acetate, 1:1); 253–254 °C; benzene; IR: $\tilde{\nu} = 3190$ (NH) and 1650 cm⁻¹ (CO); ¹H NMR ([D₆]DMSO): $\delta = 1.35$ (d, 3 H, CH₃), 4.30 (s, 2 H, CH₂), 4.70 (q, 1 H, CH), 7.30–7.37 (m, 3 H, benzene C3–H and benzyl C2–H and C6–H), 7.54 (m, 1 H, benzene C4–H), 7.67–7.70 (m, 2 H, benzene C6–H and benzyl C4–H), 10.50 ppm (br s, 1 H, NH).

General procedure for the preparation of compounds **2f,h,j,l,n,q,s,y,aa**; example: 8-chloro-2-[(2,6-difluorophenyl)methyl]-2,3-dihydro-3-methyl-1,2,5-benzothiadiazepin-4(5H)-thione 1,1-dioxide (**2y**). A solution of **2v** (400 mg, 1.0 mmol) and Lawesson's reagent (400 mg, 1 mmol) in xylene (6 mL) was stirred at 100 °C for 4 h. The solvent was removed, and the crude product was separated by chromatography on a silica gel column (chloroform as

eluent) to afford pure **2y** (200 mg, 50%); m.p. 176–177 °C (from benzene); IR: $\tilde{\nu} = 3190$ cm⁻¹ (NH); ¹H NMR (CDCl₃): $\delta = 1.70$ (d, 3 H, CH₃), 4.25 (d, 1 H, CHH), 4.63 (d, 1 H, CHH), 4.93 (q, 1 H, CH), 6.80–7.20 (m, 3 H, benzyl C3–H and C5–H and benzene C3–H), 7.32–7.41 (m, 2 H, benzyl C4–H and benzene C4–H), 7.81 (m, 1 H, benzene C6–H), 9.00 ppm (br s, 1 H, NH).

Quantity Lawesson's reagent used (equiv); yield; reaction time; melting point; recrystallization solvent; chromatographic system; IR spectroscopic data; and ¹H NMR spectroscopic data are listed for each of the following compounds:

2f: 0.5; 90%; 3 h; 172–173 °C; benzene; silica gel (chloroform); IR: $\tilde{\nu} = 3220$ cm⁻¹ (NH); ¹H NMR (CDCl₃): $\delta = 0.24$ –0.58 (m, 4 H, CH₂), 1.12 (m, 1 H, CH), 1.72 (m, 3 H, CH₃), 3.05 (dd, 2 H, N–CH₂), 4.86 (q, 1 H, CH–CH₃), 7.02 (d, $J_o = 8.7$ Hz, 1 H, benzene C3–H), 7.49 (dd, $J_o = 8.7$ Hz, $J_m = 2.5$ Hz, 1 H, benzene C4–H), 7.98 (d, $J_m = 2.5$ Hz, 1 H, benzene C6–H), 9.66 ppm (br s, 1 H, NH).

2h: 0.5; 85%; 4 h; 161–162 °C; benzene/cyclohexane; silica gel (chloroform); IR: $\tilde{\nu} = 3300$ cm⁻¹ (NH); ¹H NMR (CDCl₃): $\delta = 1.71$ (d, 3 H, CH₃), 3.91 (m, 2 H, CH₂), 4.77 (q, 1 H, CH), 5.28 (m, 2 H, =CH₂), 5.85 (m, 1 H, =CH), 7.06 (d, $J_o = 8.7$ Hz, 1 H, benzene C3–H), 7.52 (dd, $J_o = 8.7$ Hz, $J_m = 2.3$ Hz, 1 H, benzene C4–H), 7.96 (d, $J_m = 2.3$ Hz, 1 H, benzene C6–H), 9.71 ppm (br s, 1 H, NH).

2j: 1; 100%; 4.5 h; 178–179 °C; benzene; silica gel (chloroform); IR: $\tilde{\nu} = 3220$ cm⁻¹ (NH); ¹H NMR (CDCl₃): $\delta = 1.67$ (d, 3 H, CH₃), 1.83 (s, 3 H, =C–CH₃), 3.68 (d, $J_o = 16.4$ Hz, 1 H, CHH), 3.98 (d, $J_o = 16.4$ Hz, 1 H, CHH), 4.78 (q, 1 H, CH), 5.05 (d, 2 H, =CH₂), 7.07 (d, $J_o = 8.7$ Hz, 1 H, benzene C3–H), 7.53 (dd, $J_o = 8.7$ Hz, $J_m = 2.3$ Hz, 1 H, benzene C4–H), 7.98 (d, $J_m = 2.3$ Hz, 1 H, benzene C6–H), 9.50 ppm (br s, 1 H, NH).

2l: 0.5; 95%; 3 h; 159–161 °C; benzene; silica gel (chloroform); IR: $\tilde{\nu} = 3230$ cm⁻¹ (NH); ¹H NMR (CDCl₃): $\delta = 1.67$ (m, 6 H, CH₃), 3.71–4.01 (m, 2 H, CH₂), 4.77 (q, 1 H, CH), 5.45–5.79 (m, 2 H, =CH), 7.05 (d, $J_o = 8.7$ Hz, 1 H, benzene C3–H), 7.52 (dd, $J_o = 8.7$ Hz, $J_m = 2.4$ Hz, 1 H, benzene C4–H), 7.96 (d, $J_m = 2.4$ Hz, 1 H, benzene C6–H), 9.71 ppm (br s, 1 H, NH).

2n: 0.5; 86%; 2 h; 175–178 °C; benzene; silica gel (chloroform/ethyl acetate, 1:1); IR: $\tilde{\nu} = 3220$ cm⁻¹ (NH); ¹H NMR (CDCl₃): $\delta = 1.66$ (m, 9 H, CH₃), 3.86 (m, 2 H, CH₂), 4.72 (q, 1 H, CH), 5.19 (m, 1 H, =CH), 7.00 (d, $J_o = 8.7$ Hz, 1 H, benzene C3–H), 7.46 (dd, $J_o = 8.7$ Hz, $J_m = 2.2$ Hz, 1 H, benzene C4–H), 7.92 (d, $J_m = 2.2$ Hz, 1 H, benzene C6–H), 9.62 ppm (br s, 1 H, NH).

2q: 0.5; 77%; 4 h; 130–132 °C; benzene; silica gel (chloroform); IR: $\tilde{\nu} = 3230$ cm⁻¹ (NH); ¹H NMR (CDCl₃): $\delta = 1.78$ (d, 3 H, CH₃), 4.07 (m, 2 H, CH₂), 4.82 (q, 1 H, CH), 6.25 (m, 1 H, CH₂–CH=), 6.61 (d, $J_t = 15.8$ Hz, 1 H, =CH–Ar), 7.01 (d, $J_o = 8.7$ Hz, 1 H, benzene C3–H), 7.30–7.36 (m, 5 H, benzene C–H), 7.52 (dd, $J_o = 8.7$ Hz, $J_m = 2.4$ Hz, 1 H, benzene C4–H), 8.01 (d, $J_m = 2.4$ Hz, 1 H, benzene C6–H), 9.45 ppm (br s, 1 H, NH).

2s: 0.5; 82%; 6 h; 161–163 °C; ethanol; silica gel (chloroform); IR: $\tilde{\nu} = 3210$ cm⁻¹ (NH); ¹H NMR (CDCl₃): $\delta = 1.47$ (d, 3 H, CH₃–CH), 2.35 (s, 3 H, CH₃), 4.38 (d, 1 H, CHH), 4.63 (d, 1 H, CHH), 4.85 (q, 1 H, CH), 7.06–7.30 (m, 4 H, benzene C–H and benzene C3–H), 7.49–7.58 (m, 2 H, benzene C–H and benzene C4–H), 8.02 (d, $J_m = 2.4$ Hz, 1 H, benzene C6–H), 9.50 ppm (br s, 1 H, NH).

2aa: 1; 26%; 7.5 h; 169–170 °C; benzene; silica gel (chloroform); IR: $\tilde{\nu} = 3190$ cm⁻¹ (NH); ¹H NMR (CDCl₃): $\delta = 1.60$ (d, 3 H, CH₃), 4.20 (d, 1 H, CHH), 4.60 (d, 1 H, CHH), 4.90 (q, 1 H, CH), 7.10 (d, $J_o = 8.4$ Hz, 1 H, benzene C3–H), 7.30 (m, 3 H, benzyl C–H), 7.52 (dd, $J_o = 8.4$ Hz, $J_m = 2.4$ Hz, 1 H, benzene C4–H), 8.00 (d, 1 H, $J_m = 2.4$ Hz, 1 H, benzene C6–H), 9.50 ppm (br s, 1 H, NH).

8-Chloro-2,3-dihydro-2-epoxydimethylallyl-3-methyl-1,2,5-benzothiadiazepin-4(5H)-one 1,1-dioxide (**2o**): A mixture of **2m** (300 mg, 0.9 mmol) and *meta*-chloroperoxybenzoic acid (*m*-CPBA) (70%, 240 mg, 0.95 mmol) in CHCl₃ (10 mL) was stirred at room tempera-

ture for 15 h. The solution was diluted with chloroform (40 mL) and washed with a saturated solution of Na_2CO_3 (5×30 mL), and with brine (3×50 mL), in turn. The solvent was removed to obtain a mixture of four diastereomers **2o** (310 mg, 100%); IR: $\tilde{\nu}=3200$ (NH) and 1650 cm^{-1} (CO); $^1\text{H NMR}$ (CDCl_3): $\delta=1.26$ (d, 6H, CH_3), 1.60–1.76 (m, 3H, $\text{CH}_3\text{--CH}$), 2.88–2.99 (m, 2H, CH_2), 3.56–3.68 (m, 1H, CH), 4.40 and 4.77 (2 q, 1H, CH--CH_3), 7.02–7.07 (m, 1H, benzene C3–H), 7.43–7.49 (m, 1H, benzene C4–H), 7.85–7.97 (m, 1H, benzene C6–H), 8.83 ppm (br s, 1H, NH).

Ethyl 2-(2-amino-5-chlorobenzenesulfonamido)acetate (**3b**): A well-stirred solution of **3a** (31.4 g, 97 mmol) in glacial acetic acid (300 mL) was heated at 60°C . Iron powder (43.6 g, 780 mmol) was then added in portions over 30 min. After evaporation of the solvent, the residue was treated with crushed ice and ethyl acetate (3×200 mL) and the upper phases were separated. The organic extracts were collected, washed with brine (3×300 mL), and dried. Removal of the solvent gave pure **3b** (25.6 g, 90%); m.p. $108\text{--}110^\circ\text{C}$ (from benzene); IR: $\tilde{\nu}=3400$, 3300 (NH) and 1720 cm^{-1} (CO); $^1\text{H NMR}$ (CDCl_3): $\delta=1.21$ (t, 3H, CH_3), 3.75 (d, 2H, CH_2), 4.10 (q, 2H, $\text{CH}_2\text{--CH}_3$), 5.53 (br s, 1H, NH), 6.72 (d, $J_o=8.8$ Hz, 1H, benzene C3–H), 7.27 (dd, $J_o=8.8$ Hz, $J_m=2.7$ Hz, 1H, benzene C4–H), 7.65 ppm (d, $J_m=2.7$ Hz, 1H, benzene C6–H).

General procedure for the preparation of compounds **3c,k**; example: 2-(2-amino-5-chlorobenzenesulfonamido)acetic acid (**3c**). A solution of **3b** (24.5 g, 84 mmol) in ethanol/tetrahydrofuran (1:1, 400 mL) was treated with NaOH (1 N, 210 mL) and stirred at room temperature for 2 h. After evaporation of the solvent, the residue was treated with a saturated solution of NaHCO_3 . The mixture was extracted with ethyl acetate (200 mL). The organic extract was discarded, and the alkaline solution was acidified with HCl (1 N) to pH 4 and then extracted with ethyl acetate (3×200 mL). The organic extracts were collected, washed with brine (6×300 mL), and dried. Evaporation of the solvent afforded pure **3c** (21.0 g, 95%); m.p. $190\text{--}1950^\circ\text{C}$ (from ethanol); IR: $\tilde{\nu}=3260$, 3320 (NH_2), 3160 (NH) and 1710 cm^{-1} (CO); $^1\text{H NMR}$ ($[\text{D}_6]\text{DMSO}$): $\delta=3.60$ (d, 2H, CH_2), 6.07 (br s, 2H, NH_2), 6.82 (d, $J_o=8.9$ Hz, 1H, benzene C3–H), 7.28 (dd, $J_o=8.9$ Hz, $J_m=2.3$ Hz, 1H, benzene C4–H), 7.45 (d, $J_m=2.3$ Hz, 1H, benzene C6–H), 8.06 (br s, 1H, NH), 12.70 ppm (br s, 1H, OH).

Yield; reaction time; chromatographic system; melting point; re-crystallization solvent; IR spectroscopic data; and $^1\text{H NMR}$ spectroscopic data are listed for:

3k: 58%; 15 h; SiO_2 (ethyl acetate); $117\text{--}119^\circ\text{C}$; benzene; IR: $\tilde{\nu}=3040$ (OH) and 1700 cm^{-1} (CO); $^1\text{H NMR}$ ($[\text{D}_6]\text{DMSO}$): $\delta=1.50$ (d, 3H, CHCH_3), 1.60 and 1.68 (2 s, 6H, $=\text{C--CH}_3$), 3.80 and 4.10 (m, 2H, NCH_2), 4.83 (q, 1H, CHCH_3), 5.05 (m, 1H, $=\text{CH}$), 7.58–8.0 ppm (m, 3H, benzene).

8-Chloro-2,3-dihydro-1,2,5-benzothiadiazepin-4(5H)-one 1,1-dioxide (**2a**): A solution of **3c** (1.0 g, 3.8 mmol) in anhydrous THF (150 mL) was treated with EDCI (730 mg, 3.8 mmol) and 4-dimethylaminopyridine (DMAP) (460 mg, 3.8 mmol). After stirring at room temperature for 15 h, HCl (1 N, 50 mL) was added, and the mixture was extracted with ethyl acetate (3×50 mL). The organic extracts were collected, washed with brine (8×100 mL), and dried. Removal of the solvent furnished a crude product, which was separated on a silica gel column (ethyl acetate as eluent) to give **2a** (380 mg, 40%); m.p. $186\text{--}188^\circ\text{C}$ (from DMF/water); IR: $\tilde{\nu}=3280$, 3100 (NH) and 1680 cm^{-1} (CO); $^1\text{H NMR}$ ($[\text{D}_6]\text{DMSO}$): $\delta=4.19$ (s, 2H, CH_2), 7.58 (dd, $J_o=8.8$ Hz, $J_m=2.3$ Hz, 1H, benzene C4–H), 7.69 (d, $J_o=8.8$ Hz, 1H, benzene C3–H), 7.78 (d, $J_m=2.3$ Hz, 1H, benzene C6–H), 8.72 and 9.16 ppm (2 br s, 2H, NH).

General procedure for the preparation of compounds **2b,ac**; example: 8-chloro-2,3-dihydro-6-nitro-1,2,5-benzothiadiazepin-4(5H)-one 1,1-dioxide (**2b**). Compound **2a** (600 mg, 2.4 mmol) was carefully

poured into concentrated HNO_3 (15 mL). After stirring at room temperature for 2 h, the mixture was treated with crushed ice and then extracted with ethyl acetate (3×50 mL). The organic layers were collected, washed with brine (6×100 mL), and dried. The solvent was removed, and the residue was separated on a silica gel column (chloroform/ethyl acetate, 9:1 as eluent) to give **2b** (450 mg, 64%); m.p. $193\text{--}195^\circ\text{C}$ (from ethanol); IR: $\tilde{\nu}=3300$ (NH) and 1680 cm^{-1} (CO); $^1\text{H NMR}$ ($[\text{D}_6]\text{DMSO}$): $\delta=4.09$ (s, 2H, CH_2), 8.13 (d, $J_m=2.6$ Hz, 1H, benzene C6–H), 8.21 (d, $J_m=2.6$ Hz, 1H, benzene C4–H), 8.94 and 9.86 ppm (2 br s, 2H, NH).

The mixture of four diastereomers **2ac** was obtained by using a similar procedure with a reaction time of 1 h at -10°C ; 100% yield; IR: $\tilde{\nu}=3200$ (NH) and 1650 cm^{-1} (CO); $^1\text{H NMR}$ (CDCl_3): $\delta=1.28$ (d, 6H, CH_3), 1.59–1.79 (m, 3H, $\text{CH}_3\text{--CH}$), 3.26–3.39 (m, 1H, CH), 3.80 (dd, 1H, CHH), 4.43 (q, 1H, CH--CH_3), 5.20 (dd, 1H, CHH), 8.19 (d, $J_m=2.6$ Hz, 1H, benzene C4–H), 8.37 (d, $J_m=2.6$ Hz, 1H, benzene C6–H), 10.36 ppm (br s, 1H, NH).

Crystallographic data for **2w** and **2x**: *R* enantiomer **2x**: $\text{C}_{96}\text{H}_{78}\text{N}_{12}\text{O}_{18}\text{F}_{12}\text{S}_6\text{Cl}_6$; $M=2320.82$; monoclinic; space group $P2_1$ (no. 4); $a=12.713(4)$, $b=25.037(9)$, $c=15.647(4)$ Å, $\beta=99.32(2)^\circ$, $V=4915(3)$ Å³; $Z=2$; $\rho_{\text{calcd}}=1.57\text{ g cm}^{-3}$; $\mu(\text{Cu}_{\text{K}\alpha})=3.61\text{ cm}^{-1}$; $F(000)=2376$. Crystal dimensions: $0.27 \times 0.22 \times 0.13\text{ mm}^3$; single crystals of **2x**, suitable for analysis, were obtained by slow evaporation from a DMSO solution. Data collection was carried out at room temperature on a Rigaku AFC5R diffractometer with graphite-monochromated $\text{Cu}_{\text{K}\alpha}$ radiation and a rotating anode generator (12 kW). Owing to the poor quality of the crystals, the entire reflection sphere was collected for best statistics. Of 30964 reflections collected ($2\theta_{\text{max}}=124^\circ$), 7944 were considered unique ($R_{\text{int}}=0.064$) and were corrected for LP and absorption. Three standard reflections, measured after every 150, remained essentially constant throughout data collection (no decay correction was applied). The structure was solved and refined with the SIR97 program.^[49] Only the sulfur and chlorine atoms were refined anisotropically and all the hydrogen atoms were positioned geometrically (riding model). Final anisotropic refinements were carried out according to the full-matrix least-squares method, based on 4519 reflections with $F_o > 8.0\sigma(F_o)$ and 660 variable parameters (ratio 6.85:1): $R=0.075$, $R_w=0.076$, $w=\sin\theta/\lambda$, $S=2.32$. As the space group is polar, the refinement was also performed on the enantiomeric structure which converged to $R=0.078$ and $R_w=0.080$. The *R*-factor ratio test^[50] gave an *R* value of 1.0011 at the 0.005 significance level. Hence, the probability of the inverted model (*S* configuration) being correct can be rejected at the 99.5% confidence level. Maximum and minimum peaks of the final difference Fourier map: $\rho_{\text{max}}=0.66$ and $\rho_{\text{min}}=-0.58\text{ e Å}^{-3}$.

Crystallographic data for the *S* enantiomer **2w**: $\text{C}_{32}\text{H}_{26}\text{N}_4\text{O}_6\text{F}_4\text{S}_2\text{Cl}_2$; $M=773.61$; monoclinic; space group $P2_1$ (no. 4); $a=7.834(3)$, $b=28.782(4)$, $c=7.837(2)$ Å, $\beta=95.89(2)^\circ$, $V=1758(1)$ Å³; $Z=2$; $\rho_{\text{calcd}}=1.46\text{ g cm}^{-3}$; $\mu(\text{Cu}_{\text{K}\alpha})=3.36\text{ cm}^{-1}$; $F(000)=792$. Crystal dimensions: $0.52 \times 0.32 \times 0.27\text{ mm}^3$; single crystals of **2w**, suitable for analysis, were obtained by slow evaporation from a DMSO solution. Data collection was carried out at room temperature on a Rigaku AFC5R diffractometer with graphite-monochromated $\text{Cu}_{\text{K}\alpha}$ radiation and a rotating anode generator (12 kW). Of 2987 reflections collected ($2\theta_{\text{max}}=124^\circ$), 2763 were considered unique ($R_{\text{int}}=0.064$) and were corrected for LP and absorption. Three standard reflections, measured after every 150, remained essentially constant throughout data collection (no decay correction was applied). The structure was solved and refined with the SIR97 program.^[49] All the heavy atoms were refined anisotropically and all hydrogen atoms were positioned geometrically (riding model). Final anisotropic refinements were carried out according to the full-matrix least-squares method, based on 1959 reflections with $F_o > 8.0\sigma(F_o)$ and 450 varia-

ble parameters (ratio 4.35:1): $R=0.059$, $R_w=0.067$, $w=\sin\theta/\lambda$, $S=2.81$. As the space group is polar, the refinement was also performed on the enantiomeric structure which converged to $R=0.066$ and $R_w=0.074$. The R -factor ratio test^[50] gave an R value of 1.0027 at the 0.005 significance level. Hence, the probability of the inverted model (R configuration) being correct can be rejected at the 99.5% confidence level. Maximum and minimum peaks of the final difference Fourier map: $\Delta\rho_{\max}=0.63$ and $\Delta\rho_{\min}=-0.39\text{ e}\text{\AA}^{-3}$. CCDC 283422 contains the supplementary crystallographic data for this paper. These data can be obtained free of charge via www.ccdc.cam.ac.uk/data_request/cif (or from the Cambridge Crystallographic Data Centre, 12 Union Road, Cambridge CB2 1EZ, UK; fax: + (44) 1223-336-033; or e-mail: data_request@ccdc.cam.ac.uk). **Microbiology:** For the antiviral assays, all compounds were solubilized in DMSO at 200 μM and then diluted in culture medium.

Cells and viruses: MT-4 cells were grown at 37 °C in a CO_2 atmosphere (5%) in RPMI 1640 medium, supplemented with fetal calf serum (FCS, 10%), penicillin G (100 IU mL^{-1}), and streptomycin (100 $\mu\text{g}\text{mL}^{-1}$). Cell cultures were verified periodically for the absence of mycoplasma contamination with a MycoTect Kit (Gibco). Human immunodeficiency virus type 1 (HIV-1, IIIB strain) was obtained from supernatants of persistently infected cells. HIV-1 stock solutions had titers of $1.5\times 10^7\text{ mL}^{-1}$ for a 50% cell culture infectious dose (CCID_{50}).

HIV titration: Titration of HIV was performed in C8166 cells by the standard limiting dilution method (dilution 1:2, four replica wells per dilution) in 96-well plates. The infectious virus titer was determined by light-microscope scoring of syncytia after four days of incubation. Virus titers were expressed as CCID_{50} per mL.

Anti-HIV assays: The activity of the compounds against multiplication of wild-type HIV-1 in acutely infected cells was based on the inhibition of virus-induced cytopathicity in MT-4 cells. Briefly, culture medium (50 μL) containing 1×10^4 cells was added to the wells of flat-bottom microtiter trays containing 50 μL of culture medium with or without various concentrations of test compounds. Then, HIV suspensions (20 μL , each containing the appropriate amount (by CCID_{50}) to cause complete cytopathicity at day 4) were added. After incubation at 37 °C, cell viability was determined by the 3-(4,5-dimethylthiazol-1-yl)-2,5-diphenyltetrazolium bromide (MTT) method.^[51] The cytotoxicity of each test compound was evaluated in parallel with its antiviral activity and was based on the viability of mock-infected cells, as monitored by the MTT method.

RT assays: Assays were performed as previously described.^[52] Briefly, purified rRT (20–50 nm) was assayed for its RNA-dependent DNA polymerase activity in a volume of 25 μL containing Tris-HCl (50 mM, pH 7.8), KCl (80 mM), MgCl_2 (6 mM), DTT (1 mM), BSA (0.1 mgmL^{-1}), template–primer duplex: [poly(rA)–oligo(dT)_{12–18}] (0.3 μM , determined by 3'-OH end concentration), and [^3H]dTTP (10 μM , 1 Ci mmole^{-1}). After a incubation at 37 °C for 30 min, samples were spotted onto glass fiber filters (Whatman GF/C) and the acid-insoluble radioactivity was determined.

Molecular modeling: (Docking studies and molecular alignment): All molecular modeling calculations and manipulations were performed using the software packages MacroModel 7.1^[53] and AutoDock 3.0.5^[44b] running on IBM-compatible AMD Athlon 3.0 GHz workstations with the Linux operating system SUSE 9.0. For conformational analyses and for any minimization, the all-atom Amber^[54] force field was adopted as implemented in the MacroModel package.

As derivative **2w** was found to be more active than the R enantiomer, all derivatives **1–3** were modeled with the absolute S configuration when applicable. The crystal structure of **2w** was used as a template to model all the derivatives **1–3**. The NNBS was defined

by using the R82913–RT complex filed in the Brookhaven Protein Data Bank^[55] (PDB entry code: 1tvr) by selecting all the residues within 20 Å of the co-crystallized inhibitor.

All modeled compounds **1–3** were merged into the NNBS in place of the R82913 structure. The complexes obtained were then minimized with the batchmin module of MacroModel to a low gradient, allowing the relaxation of a 3-Å residue core from the ligands. Upon complex minimization, the ligands were extracted maintaining their absolute Cartesian coordinate positions. This afforded the first alignment rule (Min alignment).

The previously minimized complexes were subjected to a MD run with a simulated annealing procedure as implemented in MacroModel version 7.1, and the run was conducted as follows: each complex was energy-minimized to a low gradient. The non-bonded cut-off distances were set to 20 Å for both van der Waals and electrostatic interactions. An initial random velocity was applied to all atoms corresponding to 300 K. Three subsequent MD runs were then performed. The first was carried out for 10 ps with a time-step of 1.5 fs at a constant temperature of 300 K for equilibration purposes. The next MD was carried out for 20 ps, during which time the system was coupled to a thermal bath (150 K) with a time constant of 5 ps. The time constant represents approximately the half-life for equilibration with the bath; consequently, the second MD command caused the molecule to slowly cool to ≈ 150 K. The third and last MD cooled the molecule to 50 K over 20 ps. A final energy minimization was then carried out for 250 iterations with a conjugate gradient. Similarly to the previous minimization, during all the MD procedures described above, only the residues of a core 3 Å from the ligands were allowed to relax. Energy minimizations and MD were performed in vacuo in all cases. Again, after the MD procedure was applied, all ligands were extracted while maintaining their absolute Cartesian coordinate positions. This afforded the second alignment rule (Dyn alignment).

The binding mode of TIBO- and TBO-like derivatives **1–3** was analyzed with a docking procedure by using the program AutoDock.^[44] For the docking, a grid with spacing of 0.375 Å and with point dimensions of 60 \times 80 \times 60 was used. The grid was centered on the mass center of the experimentally bound R82913 coordinates. The Lamarckian genetic algorithm with local search (GA-LS) method was adopted using the default settings. Amber united-atom charges and solvation parameters were assigned to the protein with the program ADT (AutoDock Tools). AutoDock generated 200 possible binding conformations grouped in clusters, setting the RMSD tolerance to 1 Å. For docking assessment, the same docking protocol was used on the reference drug R82913. AutoDock successfully reproduced the bound conformation with a RMSD value of only 0.63.

Once docked based on the settings described above, derivatives **1–3** were receptor-based aligned by using the AutoDock program. To this, each molecule of the training set was docked into the NNBS. The starting conformations used for docking were those extracted from the MD runs of the minimized complexes. The first-ranked docked conformation (Best Docked conformation) and the lowest-energy conformation of the most populated cluster (Best Cluster conformation) were selected to obtain two further alignment rules for the 3D QSAR study.

GRID calculations: The interaction energies were calculated by using GRID (version 21) running on IBM-compatible AMD Athlon 3.0 GHz workstations equipped with the Linux operating system SUSE 9.0. A grid spacing of 1 Å was used, setting the grid dimensions at (Å): X_{\min}/X_{\max} 6.0/28.0; Y_{\min}/Y_{\max} -46.0/-14.0; and Z_{\min}/Z_{\max} -12.0/10.0, centered on the experimentally bound conformation of R82913. The aromatic C1= and water OH2 probes were

used to evaluate the molecular interaction fields of the modeled molecules.

GOLPE PLS analyses: PLS models were calculated with GOLPE 4.5.12^[46] running on O2 and Octane SE SGI workstations equipped with the operating system 6.5.11.

The resulting probe(s)-target interaction energies for each compound were unfolded to produce 1D vector variables for each compound, which were assembled in the so-called X matrix. This matrix was pre-treated by first using a cutoff of 5 kcal mol⁻¹ to produce a more symmetrical distribution of energy values, then by zeroing small (<0.01) variable values, and finally by removing variables with small standard deviations, with appropriate cutoff values. In addition, variables taking only two distributions were also removed. The Smart Region Definition (SRD)^[56] algorithm, as implemented in the GOLPE program, was also used. A number of seeds (1000) were selected using a D-optimal design criterion in the weight space. Structural differences between different molecules in the series are reflected in groups of variables, and therefore groups were generated around each seed in 3D space. Variables with a distance of no more than 2 Å from the seeds were included in the groups. If two neighboring groups (with a distance smaller than 10 Å) contained the same information, the groups were collapsed. The groups were used in the variable selection procedure replacing the original variables. The effect of the groups on the predictability was evaluated, and groups instead of individual variables were removed from the data file. The effect of the grouped variables on the predictability was evaluated by using a fractional factorial design (FFD) procedure. A number of reduced models (twice the number of variables) were built to remove some of the variables according to the FFD design.

The effect of dummy variables (20%) on the predictability was calculated, and only if a variable had a positive effect on the predictability larger than the effect of the average dummy variable was the variable included in the final model. The FFD selection was repeated until the r^2 and q^2 values did not increase significantly. In the FFD selection, the cross-validation was conducted with five random groups over 20 iterations and a maximum of three principal components. The models were validated by using random groups. Molecules were assigned in a random way to five groups of equal size. Reduced models were built by excluding one group at a time. The formation of the groups was repeated 20 times and with a maximum model dimensionality of three components.

Acknowledgments

Thanks go to Professor Gabriele Cruciani (Molecular Discovery) and Dr. Arthur J. Olson (Molecular Graphics Laboratory) for kindly providing the GOLPE and GRID programs and, respectively, the AutoDock program. The authors are grateful to Professor P. La Colla and his research group (University of Cagliari) for antiviral tests. Thanks to the Italian Ministero della Sanità, Istituto Superiore di Sanità, V Programma Nazionale di Ricerca sull'AIDS 2003 (grants 30F.19 and 40F.78) for financial support. Acknowledgments also go to Italian MIUR (PRIN 2004).

Keywords: antiviral agents • benzothiadiazepine • high-pressure chemistry • structure-activity relationships • viruses

[1] S. Vella, L. Palmisano, *Antiviral Res.* **2000**, *45*, 1–7.

[2] G. M. Lucas, R. E. Chaisson, R. D. Moore, *Ann. Intern. Med.* **1999**, *13*, 81–87.

- [3] S. Yerly, L. Kaiser, E. Race, J. P. Bru, F. Clavel, L. Perrin, *Lancet* **1999**, *354*, 729–733.
- [4] H. Jonckheere, J. Anné, E. De Clercq, *Med. Res. Rev.* **2000**, *20*, 129–154.
- [5] J. P. Vacca, J. H. Condra, *Drug Discovery Today* **1997**, *2*, 261–272.
- [6] J. M. Kilby, S. Hopkins, T. M. Venetta, B. Dimassimo, G. A. Cloud, J. Y. Lee, L. Alldredge, E. Hunter, D. Lambert, D. Bolognesi, T. Matthews, M. R. Johnson, M. A. Nowak, G. M. Shaw, M. S. Saag, *Nat. Med.* **1998**, *4*, 1302–1307.
- [7] V. J. Merluzzi, K. D. Hargrave, M. Labadia, K. Grozinger, M. Skoog, J. C. Wu, C.-K. Shih, K. Eckner, S. Hattox, J. Adams, A. S. Rosenthal, R. Faanes, R. J. Eckner, R. A. Koup, J. L. Sullivan, *Science* **1990**, *250*, 1411–1413.
- [8] L. A. Kohlstaedt, J. Wang, J. M. Friedman, P. A. Rice, T. A. Steitz, *Science* **1992**, *256*, 1783–1790.
- [9] R. Esnouf, J. Ren, C. Ross, Y. Jones, D. Stammers, D. Stuart, *Nat. Struct. Biol.* **1995**, *2*, 303–308.
- [10] W. Schafer, W.-G. Friebe, H. Leinert, A. Mertens, T. Poll, W. von der Saal, H. Zilch, B. Nuber, M. L. Ziegler, *J. Med. Chem.* **1993**, *36*, 726–732.
- [11] T. Miyasaka, H. Tanaka, M. Baba, H. Hayakawa, R. T. Walker, J. Balzarini, E. De Clercq, *J. Med. Chem.* **1989**, *32*, 2507–2509.
- [12] R. Pauwels, K. Andries, J. Desmyter, D. Schols, M. J. Kukla, H. J. Breslin, A. Raeymaekers, J. Van Gelder, R. Woestenborghs, J. Heykants, K. Schellekens, M. A. C. Janssen, E. De Clercq, P. A. J. Janssen, *Nature* **1990**, *343*, 470–474.
- [13] A. Gaul, X. Rabasseda, J. Castaner, *Drugs Future* **1998**, *23*, 133–141.
- [14] D. L. Romero, *Drugs Future* **1994**, *19*, 9–16.
- [15] E. De Clercq, *Med. Res. Rev.* **1993**, *13*, 229–258.
- [16] M. J. Kukla, H. J. Breslin, R. Pauwels, C. L. Fedde, M. Miranda, M. K. Scott, R. G. Sherill, A. Raeymaekers, J. Van Gelder, K. Andries, M. A. C. Janssen, E. De Clercq, P. A. J. Janssen, *J. Med. Chem.* **1991**, *34*, 746–751.
- [17] M. J. Kukla, H. J. Breslin, C. J. Diamond, P. P. Grous, C. Y. Ho, M. Miranda, J. D. Rodgers, R. G. Sherill, E. De Clercq, R. Pauwels, K. Andries, L. J. Moens, M. A. C. Janssen, P. A. J. Janssen, *J. Med. Chem.* **1991**, *34*, 3187–3197.
- [18] H. J. Breslin, M. J. Kukla, D. W. Ludovici, R. Mohrbacher, W. Ho, M. Miranda, J. D. Rodgers, T. K. Hitchens, G. Leo, D. A. Gauthier, C. Y. Ho, M. K. Scott, E. De Clercq, R. Pauwels, K. Andries, M. A. C. Janssen, P. A. J. Janssen, *J. Med. Chem.* **1995**, *38*, 771–793.
- [19] W. Ho, M. J. Kukla, H. J. Breslin, D. W. Ludovici, P. P. Grous, C. J. Diamond, M. Miranda, J. D. Rodgers, C. Y. Ho, E. De Clercq, R. Pauwels, K. Andries, M. A. C. Janssen, P. A. J. Janssen, *J. Med. Chem.* **1995**, *38*, 794–802.
- [20] R. H. Smith, Jr., W. L. Jorgensen, J. Tirado-Rives, M. L. Lamb, P. A. J. Janssen, C. J. Michejda, M. B. Kroger Smith, *J. Med. Chem.* **1998**, *41*, 5272–5286.
- [21] M. A. L. Eriksson, J. Pitera, P. A. Kollman, *J. Med. Chem.* **1999**, *42*, 868–881.
- [22] M. L. Barreca, A. Carotti, A. Carrieri, A. Chimirri, A. M. Monforte, M. Pellegrini Calace, A. Rao, *Bioorg. Med. Chem.* **1999**, *7*, 2283–2292.
- [23] J. Ding, K. Das, H. Moereels, L. Koymans, K. Andries, P. A. J. Janssen, S. H. Hughes, E. Arnold, *Struct. Biol.* **1995**, *2*, 407–415.
- [24] R. Pauwels, K. Andries, Z. Debyser, M. J. Kukla, D. Schols, H. J. Breslin, R. Woestenborghs, J. Desmyter, M. A. C. Janssen, E. De Clercq, P. A. J. Janssen, *Antimicrob. Agents Chemother.* **1994**, *38*, 2863–2870.
- [25] G. Grandolini, L. Perioli, V. Ambrogio, *Eur. J. Med. Chem.* **1999**, *34*, 701–709.
- [26] H. J. Breslin, M. J. Kukla, T. Kromis, H. Cullis, F. De Knaep, R. Pauwels, K. Andries, E. De Clercq, M. A. C. Janssen, P. A. J. Janssen, *Bioorg. Med. Chem.* **1999**, *7*, 2427–2436.
- [27] J. B. McMahon, R. J. Gulakowski, O. S. Weialow, R. Shultz, V. L. Narayanan, D. J. Clanton, R. Pedemonte, S. W. Wassmundt, R. W. Buckheit, Jr., W. D. Decker, E. L. White, J. Bader, M. R. Boyd, *Antimicrob. Agents Chemother.* **1993**, *37*, 754–760.
- [28] M. Artico, R. Silvestri, S. Massa, A. G. Loi, S. Corrias, G. Piras, P. La Colla, *J. Med. Chem.* **1996**, *39*, 522–530.
- [29] M. Artico, R. Silvestri, E. Pagnozzi, B. Bruno, E. Novellino, G. Greco, S. Massa, A. Ettore, A. G. Loi, F. Scintu, P. La Colla, *J. Med. Chem.* **2000**, *43*, 1886–1891.
- [30] R. Silvestri, M. Artico, G. De Martino, E. Novellino, G. Greco, A. Lavecchia, S. Massa, A. G. Loi, S. Doratiotto, P. La Colla, *Bioorg. Med. Chem.* **2000**, *8*, 2305–2309.
- [31] T. M. Williams, T. M. Ciccarone, S. C. MacTough, C. S. Rooney, S. K. Balani, J. H. Condra, E. A. Emini, M. E. Goldman, W. J. Greenlee, L. R. Kauffman,

- J. A. O'Brien, V. V. Sardana, W. A. Schleif, A. D. Theoharides, P. S. Anderson, *J. Med. Chem.* **1993**, *36*, 1291–1294.
- [32] R. Silvestri, G. De Martino, G. La Regina, M. Artico, S. Massa, L. Vargiu, M. Mura, A. G. Loi, T. Marceddu, P. La Colla, *J. Med. Chem.* **2003**, *46*, 2482–2493.
- [33] R. Silvestri, M. Artico, G. De Martino, G. La Regina, R. Loddio, M. La Colla, M. Mura, P. La Colla, *J. Med. Chem.* **2004**, *47*, 3892–3896.
- [34] R. Costi, R. Di Santo, M. Artico, S. Massa, *J. Heterocycl. Chem.* **2002**, *39*, 81–90.
- [35] R. Di Santo, R. Costi, M. Artico, S. Massa, M. E. Marongiu, A. G. Loi, A. De Montis, P. La Colla, *Antiviral Chem. Chemother.* **1998**, *9*, 127–137.
- [36] S. Clementi, GOLPE 4.5.12; Multivariate Infometric Analyses (MIA): Viale del Castagni 16, Perugia, Italy, **1999**; SGI.
- [37] P. J. Goodford, *J. Med. Chem.* **1985**, *28*, 849–857.
- [38] J. Okamoto, E. Yashima, *Angew. Chem.* **1998**, *110*, 1072–1095; *Angew. Chem. Int. Ed.* **1998**, *37*, 1020–1043.
- [39] R. Cirilli, R. Costi, R. Di Santo, M. Artico, A. Roux, B. Gallinella, L. Zanitti, F. La Torre, *J. Chromatogr. A* **2003**, *993*, 17–28.
- [40] L. L. C. Schrodinger, 2003. 32nd Floor, Tower 45, 120 West Forty-Fifth Street, New York, 10036.
- [41] W. Sippl, J. M. Contreras, I. Parrot, Y. M. Rival, C. G. Wermuth, *J. Comput.-Aided Mol. Des.* **2001**, *15*, 395–410.
- [42] W. Sippl, *J. Comput.-Aided Mol. Des.* **2000**, *14*, 559–572.
- [43] K. Das, J. P. Ding, Y. Hsiou, A. D. Clark, H. Moereels, L. Koymans, K. Andries, R. Pauwels, P. A. J. Janssen, P. L. Boyer, P. Clark, R. H. Smith, M. B. K. Smith, C. J. Michejda, S. H. Hughes, E. Arnold, *J. Mol. Biol.* **1996**, *264*, 1085–1100.
- [44] a) G. M. Morris, D. S. Goodsell, R. S. Halliday, R. Huey, W. E. Hart, R. K. Belew, A. J. Olson, *J. Comput. Chem.* **1998**, *19*, 1639–1662; b) D. S. Goodsell, G. M. Morris, A. J. Olson, *J. Mol. Recognit.* **1996**, *9*, 1–5; c) P. J. Lewi, M. de Jonge, F. Daeyaert, L. Koymans, M. Vinkers, J. Heeres, P. A. Janssen, E. Arnold, K. Das, A. D. Clark, Jr., S. H. Hughes, P. L. Boyer, M. P. de Bethune, R. Pauwels, K. Andries, M. Kukla, D. Ludovici, B. De Corte, R. Kavash, C. Ho, *J. Comput.-Aided Mol. Des.* **2003**, *17*, 129–134.
- [45] M. Pastor, G. Cruciani, K. A. Watson, *J. Med. Chem.* **1997**, *40*, 4089–4102.
- [46] M. Baroni, G. Costantino, G. Cruciani, D. Riganelli, R. Valigi, S. Clementi, *Quant. Struct.-Act. Relat.* **1993**, *12*, 9–20.
- [47] A. Tafi, J. Anastassopoulou, T. Theophanides, M. Botta, F. Corelli, S. Massa, M. Artico, R. Costi, R. Di Santo, R. Ragno, *J. Med. Chem.* **1996**, *39*, 1227–1235.
- [48] R. Ragno, G. R. Marshall, R. Di Santo, R. Costi, S. Massa, R. Rompei, M. Artico, *Bioorg. Med. Chem.* **2000**, *8*, 1423–1432.
- [49] A. Altomare, M. C. Burla, M. Camalli, G. L. Cascarano, C. Giacovazzo, A. Guagliardi, A. G. G. Moliterni, G. Polidori, R. Spagna, *J. Appl. Crystallogr.* **1999**, *32*, 115–119.
- [50] W. C. Hamilton, *Acta Crystallogr.* **1965**, *18*, 502–510.
- [51] R. Pauwels, J. Balzarini, M. Baba, R. Snoeck, D. Schols, P. Herdewijn, J. Desmyter, E. De Clercq, *J. Virol. Methods* **1988**, *20*, 309–321.
- [52] M. Botta, M. Artico, S. Massa, A. Gambacorta, M. E. Marongiu, A. Pani, P. La Colla, *Eur. J. Med. Chem.* **1992**, *27*, 251–257.
- [53] F. Mohamadi, N. G. J. Richards, W. C. Guida, R. Liskamp, M. Lipton, C. Caufield, G. Chang, T. Hendrickson, W. C. Still, *J. Comput. Chem.* **1990**, *11*, 440–467.
- [54] D. A. Pearlman, D. A. Case, J. W. Caldwell, W. S. Ross, T. E. I. Cheatham, S. Debolt, D. M. Ferguson, G. L. Seibel, P. A. Kollman, *Comput. Phys. Commun.* **1995**, *91*, 1–41.
- [55] H. Berman, K. Henrick, H. Nakamura, *Nat. Struct. Biol.* **2003**, *10*, 980.
- [56] M. Pastor, G. Cruciani, S. Clementi, *J. Med. Chem.* **1997**, *40*, 1455–1464.

Received: August 3, 2005